AD-A033 640 HONEYWELL CORPORATE RESEARCH CENTER BLOOMINGTON MINN F/G 20/12
ADVANCED DEVELOPMENT ON GALLIUM PHOSPHIDE MATERIALS FOR SATELLI--ETC(U)
MAY 76 P E PETERSEN, R G SCHULZE, M W SCOTT F33615-75-C-5244
UNCLASSIFIED HR-46492 AFML-TR-76-79 NL

1 OF 2
AD-A
033 640

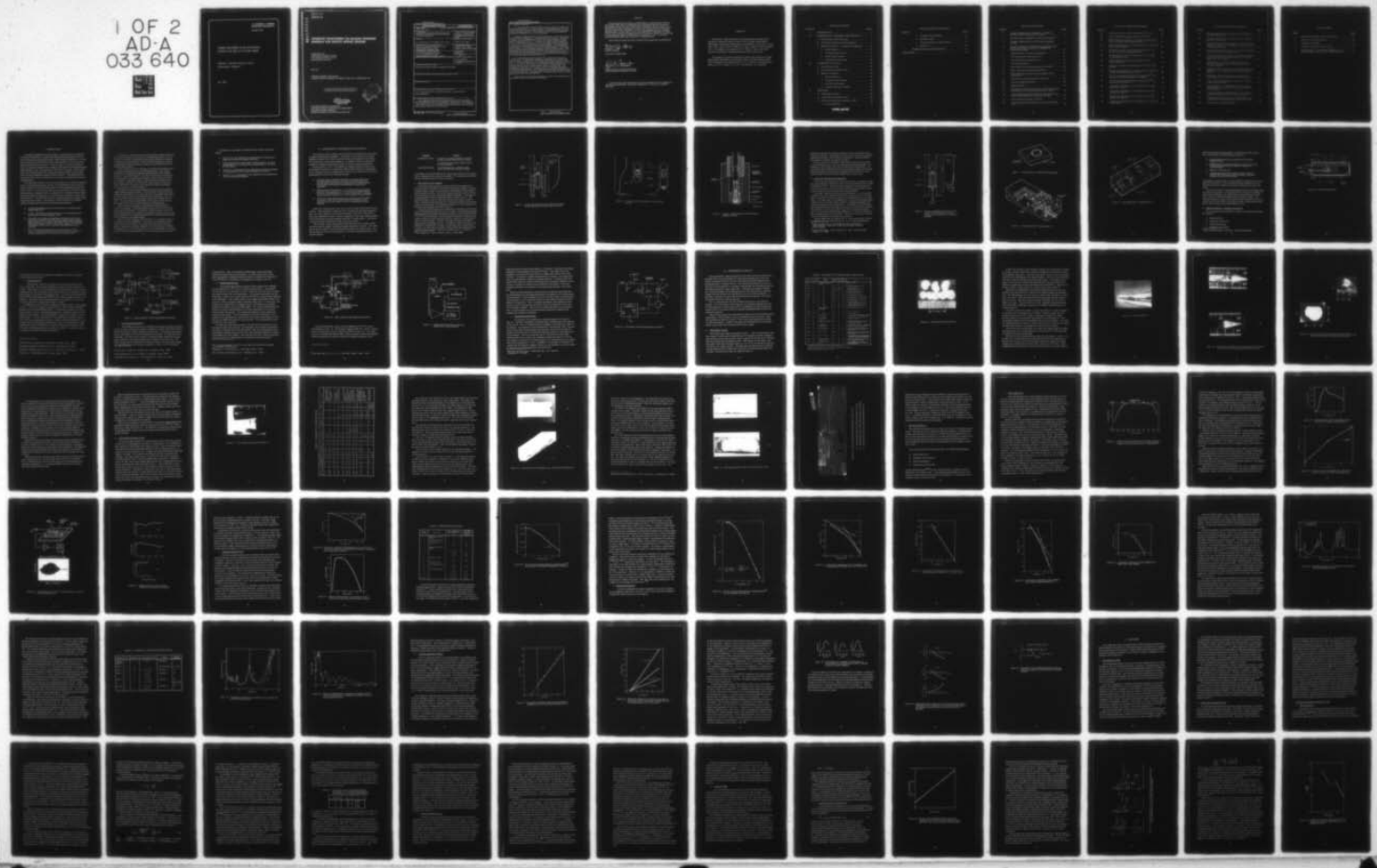

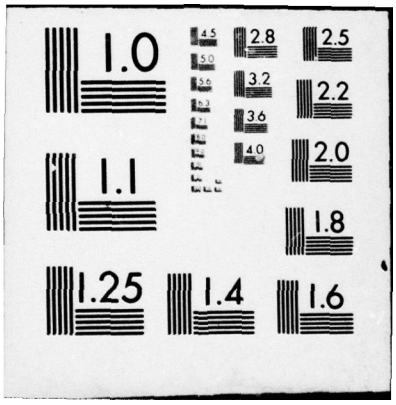
1.0
1.1
1.25
1.4
1.6
2.8
3.2
3.6
4.0
2.5
2.2
2.0
1.8

U.S. DEPARTMENT OF COMMERCE
National Technical Information Service

AD-A033 640

ADVANCED DEVELOPMENT ON GALLIUM PHOSPHIDE MATERIALS FOR SATELLITE ATTITUDE SENSORS

HONEYWELL CORPORATE RESEARCH CENTER
BLOOMINGTON, MINNESOTA

MAY 1976

AD A033640

365014

AFML-TR-76-79

ADVANCED DEVELOPMENT ON GALLIUM PHOSPHIDE MATERIALS FOR SATELLITE ATTITUDE SENSORS

HONEYWELL INC.
CORPORATE RESEARCH CENTER
10701 LYNDALE AVENUE SOUTH
BLOOMINGTON, MN 55420

MAY 1976

TECHNICAL REPORT AFML-TR-76-79
INTERIM TECHNICAL REPORT FOR PERIOD 15 MAY 1975 - 29 FEBRUARY 1976

Approved for public release; distribution unlimited

DDC
DEC 22 1976
DISTRIBUTION

REPRODUCED BY
NATIONAL TECHNICAL
INFORMATION SERVICE
U. S. DEPARTMENT OF COMMERCE
SPRINGFIELD, VA. 22161

AIR FORCE MATERIALS LABORATORY
AIR FORCE WRIGHT AERONAUTICAL LABORATORIES
AIR FORCE SYSTEMS COMMAND
WRIGHT-PATTERSON AIR FORCE BASE, OHIO 45433

UNCLASSIFIED

SECURITY CLASSIFICATION OF THIS PAGE (When Data Entered)

REPORT DOCUMENTATION PAGE		READ INSTRUCTIONS BEFORE COMPLETING FORM
1. REPORT NUMBER AFML-TR-76-79	2. GOVT ACCESSION NO.	3. RECIPIENT'S CATALOG NUMBER
4. TITLE (and Subtitle) ADVANCED DEVELOPMENT ON GALLIUM PHOSPHIDE MATERIALS FOR SATELLITE ATTITUDE SENSORS		5. TYPE OF REPORT & PERIOD COVERED Interim Technical Report 15 May 75 - 29 Feb 76
		6. PERFORMING ORG. REPORT NUMBER 46492
7. AUTHOR(s) P. E. Petersen, R. G. Schulze, M. W. Scott		8. CONTRACT OR GRANT NUMBER(s) F33615-75-C-5244
9. PERFORMING ORGANIZATION NAME AND ADDRESS Honeywell Corporate Research Center 10701 Lyndale Avenue South Bloomington, Minnesota 55343		10. PROGRAM ELEMENT, PROJECT, TASK AREA & WORK UNIT NUMBERS Project - 7371; Task - 737102; Work Unit 73710233
11. CONTROLLING OFFICE NAME AND ADDRESS Air Force Materials Laboratory Air Force Systems Command Wright Patterson AFB, Ohio 45433		12. REPORT DATE May 1976
		13. NUMBER OF PAGES 99
14. MONITORING AGENCY NAME & ADDRESS(if different from Controlling Office)		15. SECURITY CLASS. (of this report) UNCLASSIFIED
		15a. DECLASSIFICATION/DOWNGRADING SCHEDULE

16. DISTRIBUTION STATEMENT (of this Report)

Approved for public release, distribution unlimited.

17. DISTRIBUTION STATEMENT (of the abstract entered in Block 20, if different from Report)

18. SUPPLEMENTARY NOTES

19. KEY WORDS (Continue on reverse side if necessary and identify by block number)

III-V Compounds, GaP, Liquid Phase Epitaxy, Solution Growth, Photoconductivity

20. ABSTRACT (Continue on reverse side if necessary and identify by block number)

The objective of this research program is to develop the solution-growth technology of GaP so that crystals of sufficient size and uniformity can be produced for Air Force photodetector applications. To accomplish this objective two growth techniques, bulk solution growth (BSG) and liquid phase epitaxy (LPE) have been developed.

DD FORM 1 JAN 73 1473 EDITION OF 1 NOV 65 IS OBSOLETE

UNCLASSIFIED

SECURITY CLASSIFICATION OF THIS PAGE (When Data Entered)

20. Abstract (continued)

An LPE growth system which utilizes a six-bin slider in an isothermal furnace was developed. An important feature of this apparatus is the use of forced cooling of the LPE substrate holder to establish a temperature gradient at the growth interface. The final form of the LPE system produces specularly reflecting 12.7 mm x 4.8 mm layers.

Undoped and copper doped LPE layers were grown. These layers were characterized by standard C-V and photoconductivity analysis. The spectral response of the photoconductivity of these LPE layers exhibits the broad spectral response (2.25 to 3.8 eV) typical of as-grown solution grown surfaces. Photoconductive gains $\sim 2 \times 10^4$, which imply that the $\mu\tau$ product is $\sim 10^{-2}$ cm^2/V, have been measured in these samples. The photoconductive response time at low levels of illumination is typically a few milliseconds. A $\mu\tau$ product of 10^{-2} translates to a majority carrier lifetime $\sim 10^{-4}$ second. Hence majority carrier trapping effects are minimal in this material. The photosignal varies linearly with photon flux in the region from 10^{-11} to 10^{-13} photons/cm^2 sec and sublinearly ($\sim F^{1/2}$) at higher photon flux densities. The spatial uniformity of the photosignal in LPE GaP:Cu has been measured to be less than ±10% over distances of 0.2 cm.

In the bulk solution growth technique GaP is dissolved at the top of a crucible of Ga, the phosphorus transports by diffusion to the bottom of the crucible which is cooler, and a GaP crystal grows from the saturated solution. A BSG growth apparatus was developed with which large area (~ 6 mm ϕ) crystals of GaP have been grown. Hall analysis of these crystals shows that the majority carrier concentration is uniform to within ±10%. The temperature dependence of the mobility of both n- and p-type BSG grown samples has been measured. IR spectroscopy and oscillatory photoconductivity and Hall analysis has been used to identify the principal impurities in both n- and p-type BSG GaP. Photocapacitance techniques have been used to study deep levels in both BSG and LPE GaP.

In summary the LPE and BSG processes have been successfully used for the growth of large area uniform GaP crystals.

NOTICE

When Government drawings, specifications, or other data are used for any purpose other than in connection with a definitely related Government procurement operation, the United States Government thereby incurs no responsibility nor any obligation whatsoever; and the fact that the Government may have formulated, furnished, or in any way supplied the said drawings, specifications, or other data, is not to be regarded by implication or otherwise as in any manner licensing the holder or any other person or corporation, or conveying any rights or permission to manufacture, use, or sell any patented invention that may in any way be related thereto.

This technical report has been reviewed and is approved for publication.

Robert J. Sprry

ROBERT J. SPRY
Project Monitor

FOR THE COMMANDER

W G D Frederick

WILLIAM G. D. FREDERICK
Chief
Laser and Optical Materials Branch
Electromagnetic Materials Division

Copies of this report should not be returned unless return is required by security considerations, contractual obligations, or notice on a specific document.

AIR FORCE - 8 NOVEMBER 76 - 200

PREFACE

This interim report describes work performed by personnel of the Honeywell Corporate Research Center, 10701 Lyndale Avenue South, Bloomington, Minnesota 55420 during the period from 15 May 1975 - 29 February 1976, under Contract F33615-75-C-5244, Project FY1457-75-02042/7371. The program was monitored by Dr. Robert J. Spry, Air Force Materials Laboratory, Wright-Patterson Air Force Base, Ohio.

The program was directed toward the growth and evaluation of copper doped gallium phosphide by liquid phase epitaxy and bulk solution growth. This investigation was conducted by Dr. P. E. Petersen, principal investigator, Mr. R. G Schulze, Dr. M. W. Scott and Mr. S. R. Peterson.

TABLE OF CONTENTS

SECTION		PAGE
I	INTRODUCTION	1
II	EXPERIMENTAL TECHNIQUES AND APPARATUS	4
	A. Bulk Solution Growth Apparatus	5
	B. Liquid Phase Epitaxial Growth Apparatus	9
	C. Material Evaluation - Techniques and Apparatus . . .	13
	1. Photoconductivity	15
	2. Transport Measurements	15
	3. Infrared Spectroscopy	17
	4. Capacitance Spectroscopy	20
III	EXPERIMENTAL RESULTS	22
	A. Bulk Solution Growth	22
	B. Liquid Phase Epitaxial Growth	30
	C. Material Evaluation	38
	1. Photoconductivity	39
	2. Transport Measurements	45
	3. Infrared Spectroscopy	49
	4. Junction Capacitance Studies	61
IV	DISCUSSION	68
	A. Bulk Solution Growth	68
	B. Liquid Phase Epitaxial Growth.	69
	C. Electrical and Optical Properties of GaP	70
	1. Photoconductivity	70

Preceding page blank

TABLE OF CONTENTS (Continued)

SECTION		PAGE
	2. Transport Measurements	75
	3. IR Spectroscopy	78
	4. Junction Capacitance Measurements	79
	5. Summary	86
V	PROGRESS AND ACCOMPLISHMENTS	87
REFERENCES		89

LIST OF ILLUSTRATIONS

FIGURE		PAGE
1	Furnace configuration and temperature profile for the BSG process using a quartz crucible	6
2	Alternate growth techniques for bulk solution growth	7
3	Furnace configuration for the BSG using a graphite crucible	8
4	Furnace configuration and temperature profile for the BSG process using a cooling jet to establish the temperature gradient	10
5	Common-source substrate LPE apparatus	11
6	LPE growth slider mechanism No. 2	11
7	LPE growth slider mechanism No. 3	12
8	LPE growth apparatus	14
9	Photoconductivity measuring apparatus schematic	16
10	High-resistivity Hall apparatus schematic	18
11	Photoconductivity system used with Digilab FTS-14 spectrometer	19
12	Capacitance-measuring apparatus schematic	21
13	Sections of ingot from BSG-4	24
14	Ingot from BSG-7	26
15	BSG growth (a) before and (b) after removal from quartz crucible; note in (a) that growth initiated at the tip	27
16	A GaP crystal (a) and GaP wafer (b) from BSG-10; note lack of grain boundaries and gallium inclusions	28
17	GaP crystal from growth run BSG-17	31
18	Layers from (a) LPE growth run 1 and (b) LPE growth run 7	34

LIST OF ILLUSTRATIONS (Continued)

FIGURE		PAGE
19	LPE layers from (a) LPE 11-68 and (b) LPE 11-70	36
20	Surface smoothness measurement of LPE 11-66	37
21	Relative spectral response as a function of photon energy for an LPE-grown GaP:Cu photoconductor	40
22	Photoconductive gain versus photon energy for LPE 11-69 GaP:Cu photoconductor	42
23	Photocurrent versus radiation flux intensity at 2.7 eV for LPE 11-69 GaP:Cu photoconductor	42
24	Photoresponse of a GaP:Cu photoconductor to a slowly traveling photon beam	43
25	Spatial uniformity of three photoconductors from LPE 11-69 GaP:Cu	44
26	Frequency response of photoconductor from LPE 11-69 GaP:Cu	46
27	Relative photoresponse as a function of photon energy for a lapped and polished BSG-10 surface	46
28	Carrier concentration divided by (temperature)$^{3/2}$ as a function of reciprocal temperature for BSG-7	48
29	Carrier concentration divided by (temperature)$^{3/2}$ for two samples from BSG-10	50
30	Temperature dependence of the mobility for an n-type sample from BSG-10	51
31	Temperature dependence of the mobility for an n-type sample from BSG-15	52
32	Temperature dependence of the mobility for a p-type sample from BSG-10	53
33	Temperature dependence of the mobility for a LPE 10-62 n-type sample	54

LIST OF ILLUSTRATIONS (Continued)

FIGURE		PAGE
34	Absorption spectrum as a function of wave number for GaP containing S and Si	56
35	Absorption coefficient as a function of wave number for BSG-10 at 82°K and 5°K	59
36	Relative photoconductive response as a function of wave number for BSG-4 at 7°K showing the oscillatory behavior of the photoconductivity	60
37	Reciprocal capacitance squared as a function of potential for a reverse-biased Schottky barrier	62
38	Reciprocal capacitance squared as a function of potential for three reverse bias Schottky barriers on an angle lapped LPE 10-63 surface	63
39	Conductance as a function of temperature at three different frequencies for a GaP/Au Schottky barrier on a BSG substrate	65
40	Dependence of the capacitance on the energy of the probe radiation at three frequencies in a GaP/Au Schottky barrier	66
41	Dependence of the capacitance on the energy of the probe radiation for an LPE GaP/Au Schottky barrier	67
42	Energy of the photoconductivity minima as a function of the minimum number	80
43	Band schematic of a Schottky barrier and the corresponding space charge distribution for three different bias conditions	82
44	Frequency divided by $(\text{temperature})^{3/2}$ as a function of reciprocal temperature for two Schottky barriers	84
45	Equilibrium band schematic of a Schottky diode on an n-type substrate with deep donor and acceptor states	85
46	Defect levels in gallium phosphide	86

LIST OF TABLES

TABLE		PAGE
1	Summary of GaP BSG Crystal Growth Runs	23
2	Summary of LPE Growth Runs	32
3	Tabulation of Hall Data	47
4	Summary of Impurities Found in GaP	58
5	Average Value, $\bar{x}$, and Standard Deviation, S, for the Photosignal in Three GaP:Cu Photoconductors	74

I. INTRODUCTION

The gallium phosphide research program at Honeywell has established the technical feasibility of using copper-doped gallium phosphide (GaP:Cu) for the fabrication of high-performance visible radiation detectors. We have shown that these detectors can meet the requirements of the Air Force for space attitude reference systems. However, prior to research conducted under the program reported here, problems still existed in obtaining adequate reproducibility, size, and uniformity of the GaP:Cu crystals. These limitations were primarily due to the random nucleation solution growth method which had been employed during the initial research. This growth process was selected for the early research due to its lack of complexity and ease of implementation.

The long-range objective of the current program is to further develop the GaP:Cu crystal growth process so that it can reproducibly yield material of quality suitable for the high-performance detector applications specified by the Air Force. To achieve this objective we have elected to further develop solution-growth techniques which, in addition to the excellent detector characteristics already demonstrated, have the potential to yield the required size and uniformity. It is well known that the Czochralski growth technique yields large-area GaP crystals. Our decision to further advance the solution-growth techniques was based on the following considerations:

- Excellent photoproperties had been observed in solution-grown copper-doped GaP.
- To date, all reports of photoconductivity in non-solution-grown GaP:Cu give very long response times.
- GaP grown by the liquid encapsulated Czochralski (LEC) technique is not suitable for the direct fabrication of light-emitting diodes (LEDs), but is used as substrate material for subsequent liquid phase epitaxy (LPE) or vapor phase epitaxy (VPE) growth. The junction for the LED is formed in the epitaxially grown material.
- Even if adequate photoproperties could be achieved in LEC GaP:Cu a significant research effort would still be required to develop reproducibility and uniformity with that process.

To summarize, we believe it is easier to develop the solution-growth process to achieve larger size, uniformity, and reproducibility than it is to develop the LEC process to yield desired photoconductor properties in addition to uniformity and reproducibility. The fact that high-purity defect-free GaP is required for avalanche photodiode development is an additional reason for pursuing solution growth.

We have therefore elected to develop two complementary solution-growth techniques: bulk solution growth and liquid phase epitaxy. Bulk solution growth (BSG) is a phosphorous-diffusion-controlled growth from a gallium solution in a temperature gradient. We believe that this process will enable us to grow larger, more uniform photosensitive crystals than were heretofore available. Liquid phase epitaxy, a growth process with which we have had substantial experience, was selected for study because of its inherent ability to provide the as-grown surfaces which have shown very desirable ultraviolet response in our past research.

The research on these two growth approaches performed in the present program has proceeded on schedule. We have designed, built and iteratively modified the BSG apparatus to the point where the crys'al-growth parameters necessary to achieve the crystal size objectives are understood. The growth apparatus will be modified to allow growth of GaP from the synthesis of Ga and P. The uniformity and reproducibility of this synthesis solute diffusion (SSD) grown GaP:Cu will be studied during the continuing program.

Our LPE growth process has been significantly improved during the course of the program. Substantial improvements in LPE layer smoothness and size have been obtained. Photoconductive measurements on our GaP:Cu LPE layers indicate that the objectives for sensitivity, spectral response, and uniformity will be met. Reproducibility and effect of solution grown substrates will be studied in the continuing program.

While the primary emphasis in the first phase of the program has been on controlling the crystal morphology, we have also done considerable work in the area of material evaluation. Our experimental apparatus has been upgraded to improve our evaluation capability. We have developed two additional techniques for the study of defect levels in GaP. When feasible, we have measured the electronic and photoproperties of the material which we have grown.

The balance of this report is contained in four major sections as follows:

- Section II is a description of the experimental techniques and apparatus employed throughout this work.
- Section III gives the experimental results obtained. We have purposefully tried to refrain from interpretation of the results in this section.
- Section IV is a discussion of the significance and where possible an interpretation of the results presented in Section III.
- Section V is a recapitulation of the significant accomplishments achieved during this program.

II. EXPERIMENTAL TECHNIQUES AND APPARATUS

The objective of this program was to develop a new process for the growth of copper-doped gallium phosphide. Therefore, it was necessary to spend a significant fraction of the time in this first part of the program in the design and construction of the growth apparatus. In addition, work was required to upgrade the experimental apparatus which is used for material evaluation.

Solution growth, that is, precipitation of single-crystal GaP from a saturated gallium solution at a temperature 300 to 500°C below the melting point of the compound, was very deliberately selected at the inception of our GaP:Cu photoconductor work for the following reasons:

- The large body of scientific literature on photoluminescence and electroluminescence in GaP (and also GaAs) shows that solution-grown material and junctions made in solution-grown material have the smallest concentrations of defects and impurities.
- Experimental and theoretical determinations of the phase diagrams for GaP show that the Ga vacancy concentration (which has been correlated with nonradiative "killer center" concentration) decreases by 10^3 from the melting point of GaP to 1100°C.
- Previously reported photoconductive measurements in GaP:Cu prepared by other than solution growth methods have shown response times much longer than the corresponding electron lifetimes.

During the initial phases of this work we grew single-crystal GaP:Cu from solution. Photoconductors made from these crystals had high photoconductive gain, but most important, the measured response times were much shorter than those reported by others in GaP:Cu prepared by other than solution growth. We have therefore pursued remaining uniformity, reproducibility, and crystal size problems with improved versions of solution growth.

Two methods, bulk solution growth (BSG) and liquid phase epitaxy (LPE), have been used to prepare undoped and copper-doped GaP crystals. The rationale for the two aspects of this crystal growth program are shown below. The two methods are not seen as alternatives but as two interdependent parts of the growth program.

Technique	Purpose
Bulk Solution Growth	To provide a possible method for the growth of large, uniformly doped GaP:Cu crystals.
	To provide low-flaw-density single crystals for LPE substrates.
Liquid Phase Epitaxy	To provide large-area, uniformly doped GaP:Cu crystals with "as-grown" surfaces.

A description of the growth apparatus for each of these methods and the evaluation of its design and use is given in this section. The techniques and equipment used for evaluating the GaP crystals is also given.

A. Bulk Solution Growth Apparatus

The solution growth process we used previously for the preparation of GaP:Cu employed a cool-down cycle without a temperature gradient. This type of growth process results in the nucleation of many different crystal platelets within the gallium solution. We are now using an improved version of this solution growth process to grow copper-doped gallium phosphide. A schematic of the growth apparatus and its temperature profile is shown in Fig. 1. This improved technique, which we label bulk solution growth (BSG), provides a solute concentration gradient produced by a temperature gradient as the driving force for crystal growth. Two alternative procedures for the incorporation of phosphorus into the gallium are shown in Fig. 2.

The quartz growth crucibles were cleaned with a hydrofluoric acid etch and rinsed with deionized distilled water prior to loading. After placing the gallium, gallium phosphide (and copper if used) into the quartz crucible it was evacuated to $\sim 10^{-6}$ Torr and sealed off. One of the problems encountered with the use of a quartz crucible is that the GaP ingot bonds very tightly to it, requiring a HF etch to remove the quartz. Further, on cool down the differential thermal expansion causes cracking of the GaP. An additional concern with quartz is the possibility of contamination by silicon, an electrically active shallow donor to the GaP. For these reasons a graphite crucible system was designed and procured from Poco Graphite.[a] This system is shown in Fig. 3. Note that

[a] Poco Graphite Inc., 1601 S. State St., Decatur, Texas 76234.

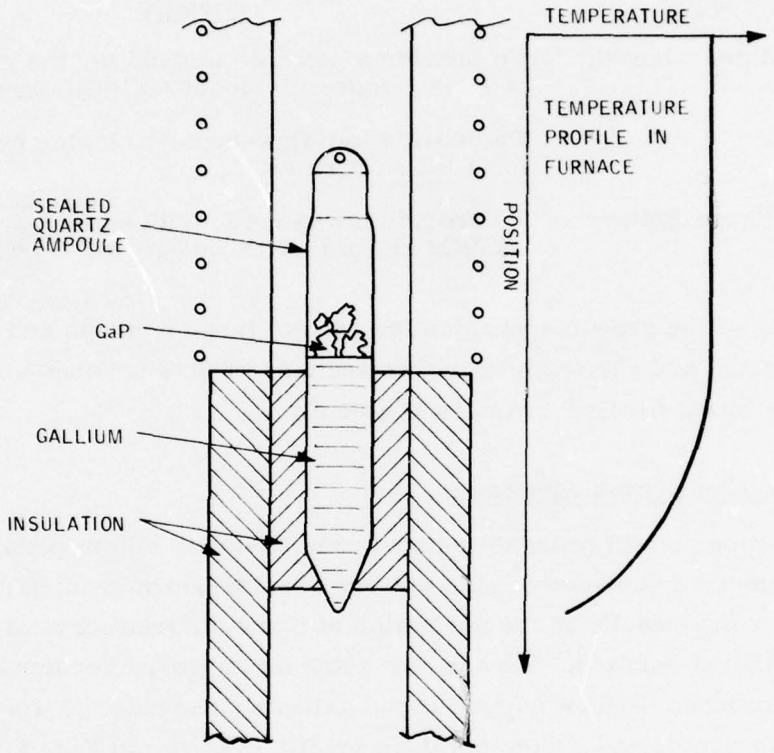

Figure 1. Furnace configuration and temperature profile for the BSG process using a quartz crucible.

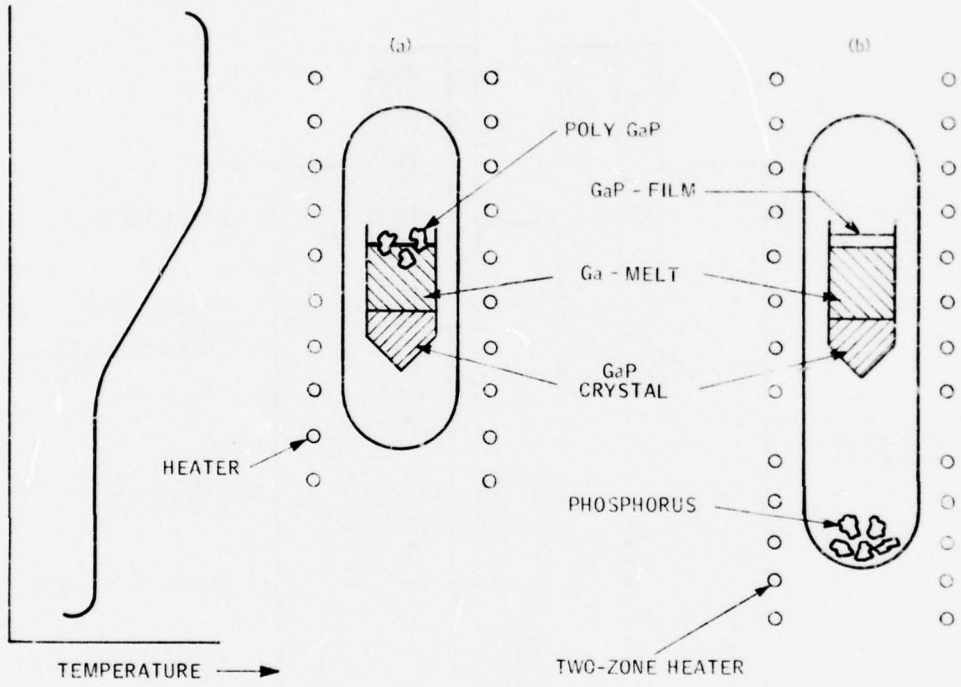

Figure 2. Alternate growth techniques for bulk solution growth.

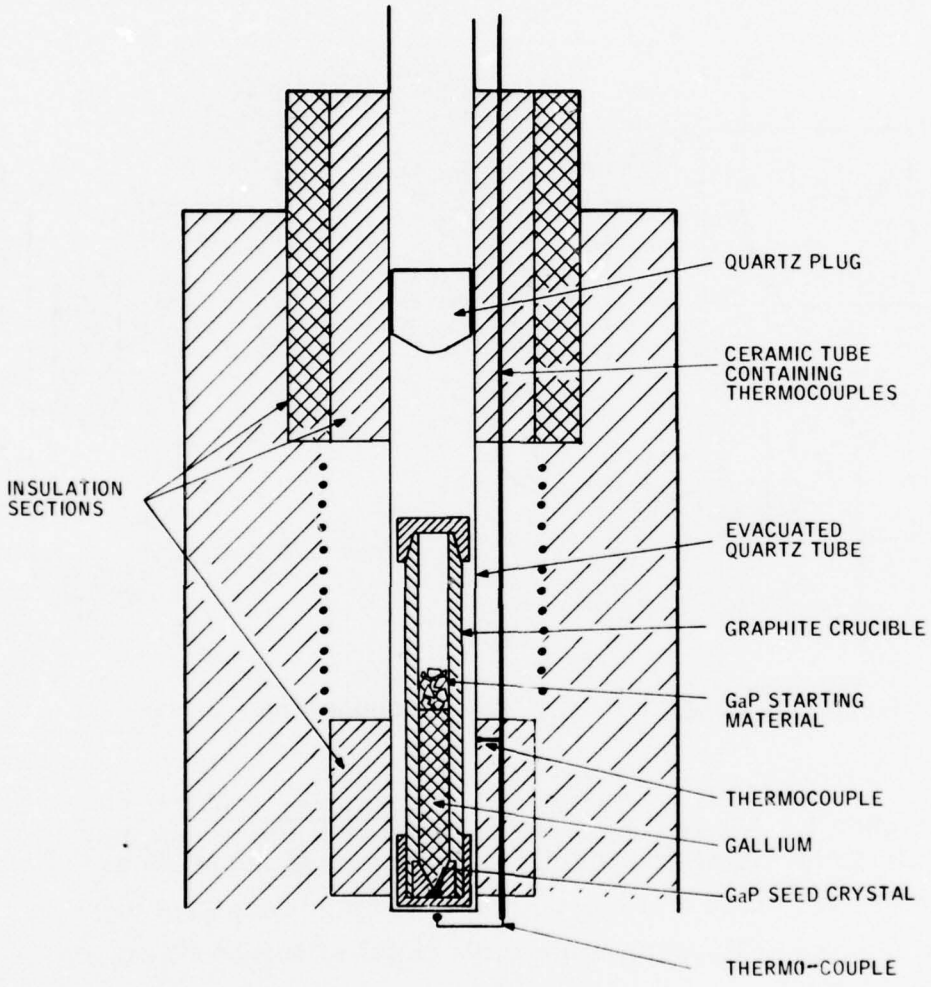

Figure 3. Furnace configuration for the BSG using a graphite crucible.

provision is also made for using a seed crystal to ensure nucleation on a preselected crystal plane. The graphite crucible must be used in an evacuated and sealed quartz ampoule, since it cannot be sealed itself. Growths took place for periods of a few days to as long as 10.5 days.

After a number of runs had been made it became clear that the heat flow in the Ga-GaP solution was such as to encourage polycrystalline growth. The modification shown in Fig. 4 was made to correct the heat flow pattern. The main feature of this configuration is that the temperature gradient in the growth charge is produced not by a temperature gradient in the furnace core, but by forced cooling of the tip of the growth ampoule with a stream of air.

B. Liquid Phase Epitaxial Growth Apparatus

Two LPE growth methods were used, a common-source substrate technique and a slider technique, although only a few runs were made with the first, which is illustrated in Fig. 5. With this method a single piece of Czochralski GaP acts both as the source of GaP to saturate the Ga during heat up and as the substrate on which LPE crystal growth occurs during cool down.

The slider method was used for all the remaining runs. One of the slider mechanisms (No. 2)[a] employed in this technique is shown in Fig. 6. All of the parts are machined from pyrolytic graphite stock obtained from Union Carbide Corp.[b] The slider works in the following way: Ga and GaP (and copper dopant if used) are put in the growth charge chambers, and lapped and polished GaP substrates are placed in the substrate slots. The sliding member (the middle one) is positioned so that the growth charge columns are not over the substrates. The assembly is raised to about 1000°C in an inert or reducing atmosphere. After the system has reached thermal equilibrium, the slider is moved to position the growth charge over the substrate. The furnace is cooled at 2°C/hr for a time corresponding to the desired layer thickness.

Another slider system is shown in Fig. 7. This mechanism (No. 3) which we designed was built by Poco Graphite Inc. from a special semiconductor

[a] Slider mechanism No. 1 was designed and constructed during an earlier program. Sliders Nos. 2 and 3 are improved versions of this first design.

[b] Union Carbide Corp., Carbon Products Div., 120 S. Riverside Plaza, Chicago, Ill. 60606.

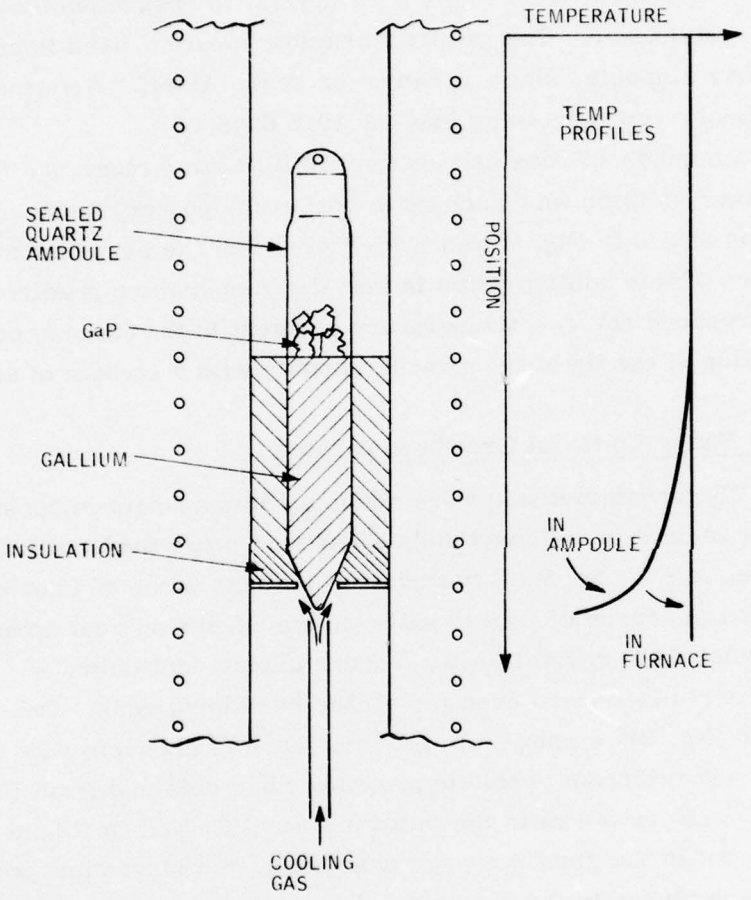

Figure 4. Furnace configuration and temperature profile for the BSG process using a cooling jet to establish the temperature gradient.

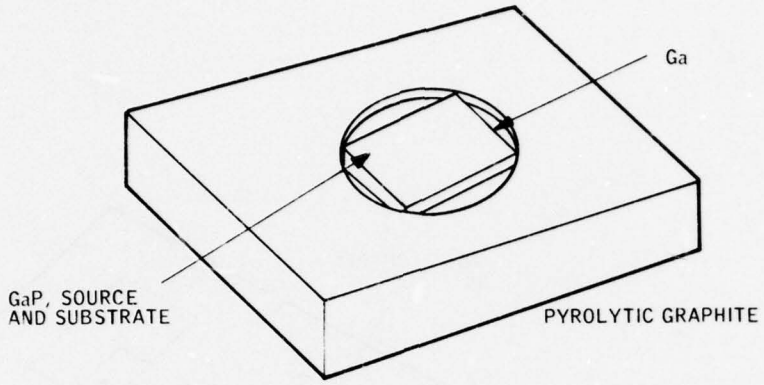

Figure 5. Common-source substrate LPE apparatus.

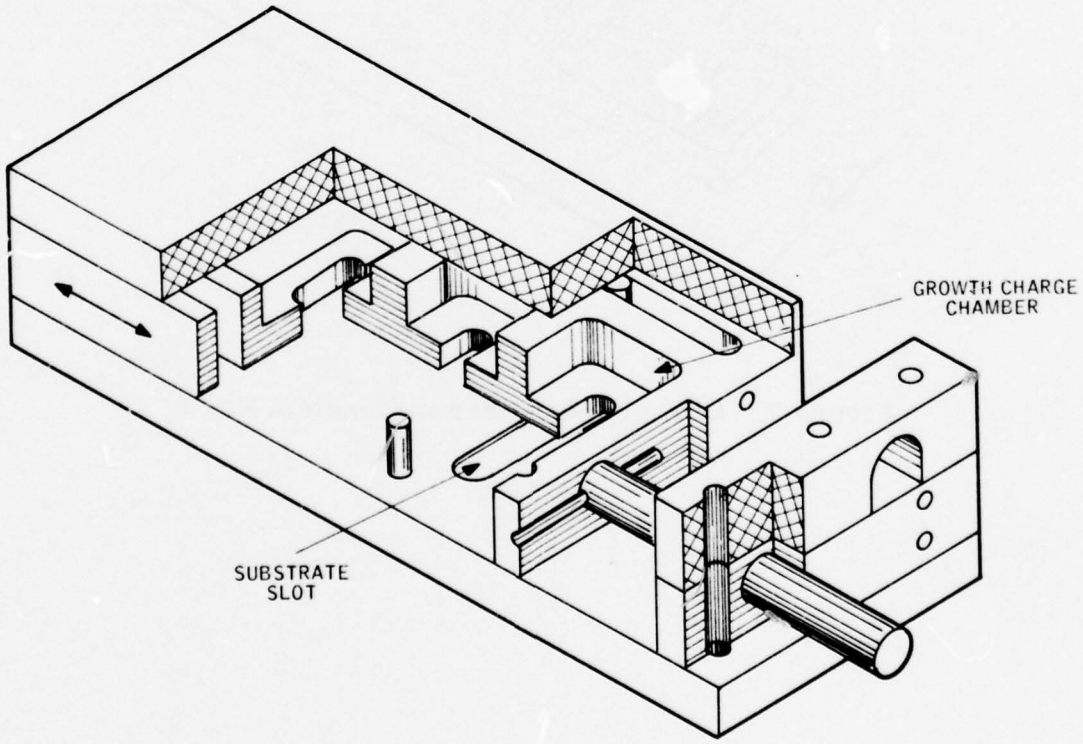

Figure 6. LPE growth slider mechanism No. 2.

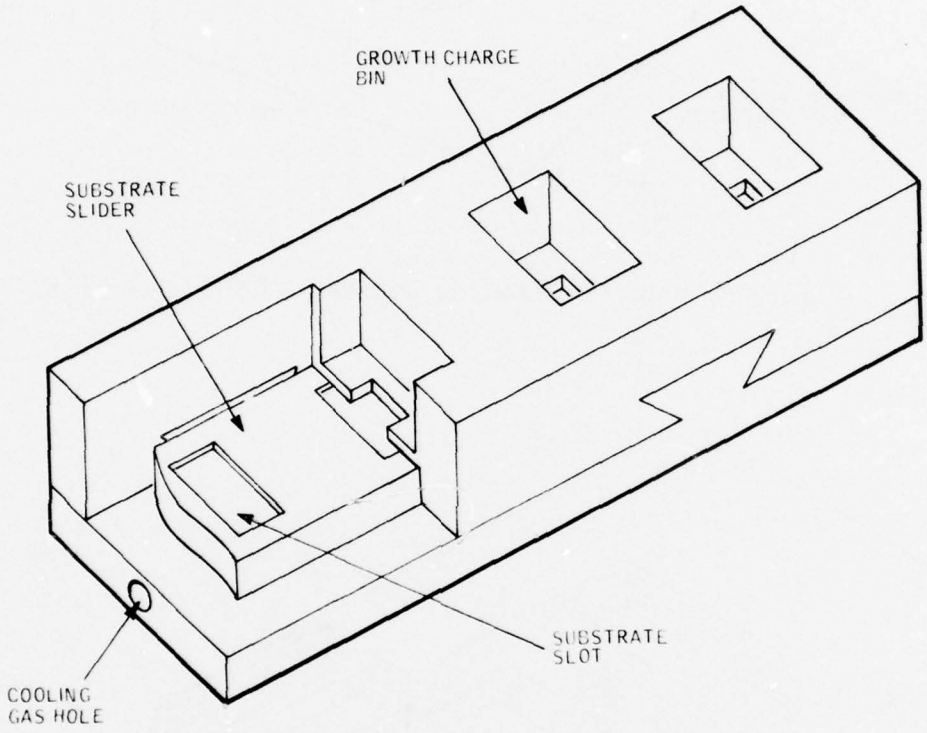

Figure 7. LPE growth slider mechanism No. 3.

grade of high-density isotropic graphite. Compared to the slider shown in Fig. 6 it incorporates the following improved features:

- Isotropic graphite which is less fragile than the pyrolytic graphite now used.
- Freedom from the constraints imposed by the very large anisotropic thermal conductivity and expansion coefficient of pyrolytic graphite.
- Capacity for six substrates.
- A cooling cavity located in the graphite directly below the substrate slots which will be used to establish a temperature gradient across the growth interface.

The addition of a cooling cavity is the most significant improvement in the design of this new slider. A well-controlled temperature gradient across the substrate-melt growth interface is necessary for the growth of smooth LPE layers.

The furnace growth tube and associated fittings were also redesigned during the course of the program. A new single-ended (to minimize the possibility of leaks) Coors[a] alumina tube was placed inside a special stainless steel alloy tube. This alloy, RA333, will withstand cyclic operation to 1100°C. The stainless steel tube is a safety feature which prevents an explosion in the event the alumina tube cracks while using a high-percentage hydrogen growth atmosphere. This system is shown schematically in Fig. 8.

C. Material Evaluation - Techniques and Apparatus

We are using four major techniques to evaluate the material grown during this program:

- Photoconductivity
- Transport measurements
- Infrared spectroscopy
- Capacitance spectroscopy

[a] Coors Porcelain Company, 600 9th St., Golden, Colorado 80401.

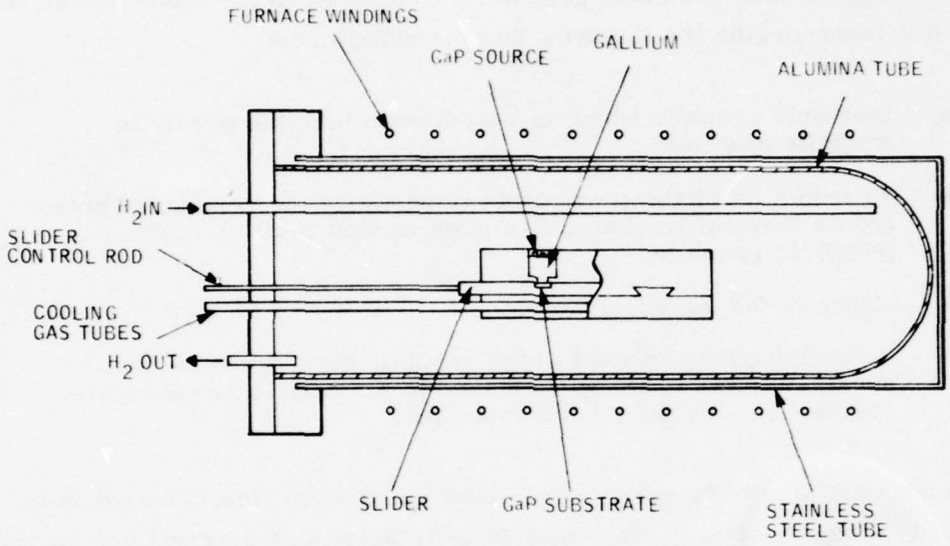

Figure 8. LPE growth apparatus.

This section discusses the techniques and apparatus generally employed in each of these measurements.

1. Photoconductivity

GaP samples, grown from solution, are generally oriented in the <1,1,1> direction. We used the phosphorous surface for photoconductivity studies. This surface is easily distinguished from the gallium surface because a polishing etch such as potassium ferrocyanide polishes the phosphorous side while putting a matte finish on the gallium side. We used the alloyed Ag:Te/Ni contact which was developed earlier[1][2] for the low-resistance contact to the material. The active area of the photoconductor was defined by the contacts in the so-called "slit" configuration (length >> width).

The apparatus used in the photoconductivity studies is shown schematically in Fig. 9. A Xenon arc lamp in conjunction with a Perkin Elmer Model 98[a] spectrometer is the illumination source. The sample is mounted on a three-way translation stage in a shielded light-tight box. Reflecting optics focus the radiation on the sample. The photoconductive signal can be read out in three different ways. The d-c photocurrent is measured with a Keithley[b] electrometer. For an a-c photomeasurement, a current-sensitive preamplifier in conjunction with a PAR-124 lock-in amplifier is used. The response to a single radiation pulse can be displayed on a storage oscilloscope by using the PAR-114[c] signal conditioning amplifier to amplify the signal. The optical system is calibrated with a EG&G[d] calibrated photodiode.

---

[a] Perkin Elmer Corporation, Main Avenue, Norwalk, Conn. 06856

[b] Keithley Instruments, 28775 Aurora Rd., Cleveland, Ohio 44139

[c] Princeton Applied Research Corp. P. O. Box 2565, Princeton, N. J. 08540

[d] EG&G Inc., 160 Brookline Ave., Boston, Mass. 02215

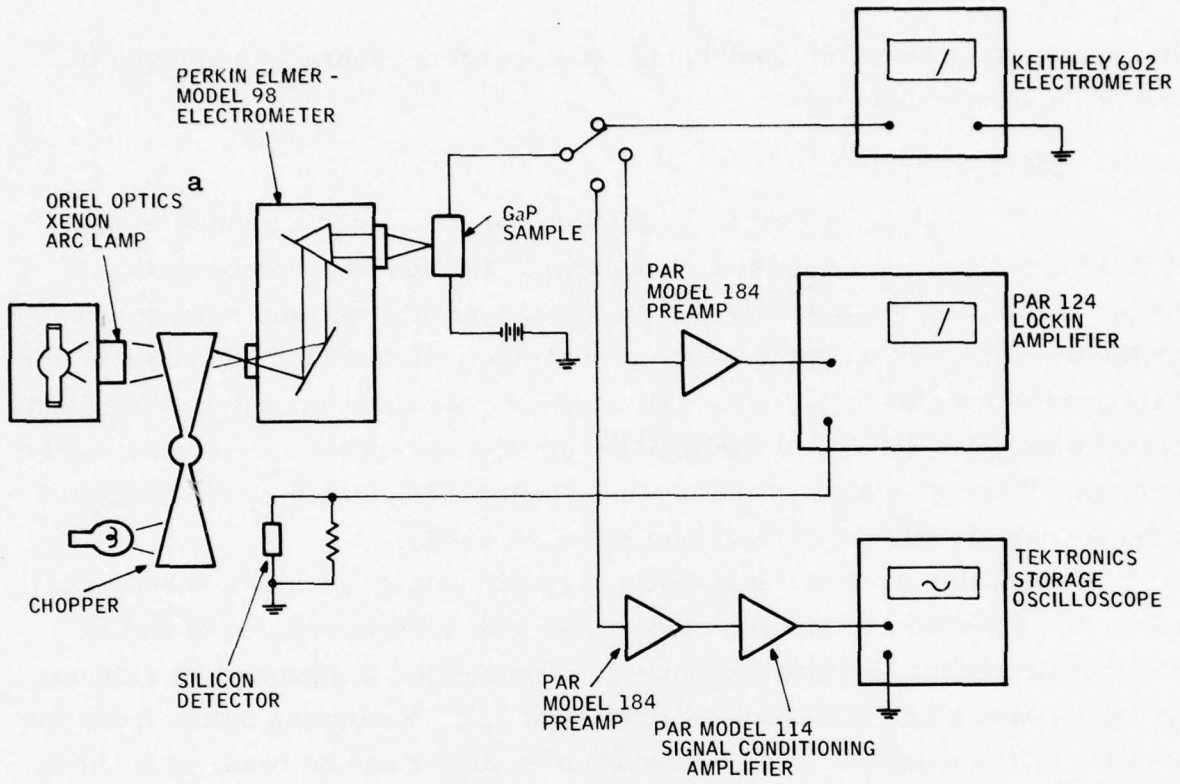

Figure 9. Photoconductivity measuring apparatus schematic.

2. Transport Measurements

Three different systems are available for Hall and resistivity analysis. In each of these systems the sample is mounted in a Janis[b] Model 8DT research dewar which can be cooled to liquid He temperature. The sample temperature can be controlled to 0.1°K with a Lakeshore Cryotronics[c] DT-500 temperature controller. The first system requires a standard bridge-shaped Hall sample and is capable of measuring samples with resistances up to 10^9 ohms. To enable measurement of samples with arbitrary shapes, we constructed, during this reporting period, the necessary apparatus to make van der Pauw Hall

[a]Oriel Corp. of America, 15 Market St., Stamford, Conn. 06902

[b]Janis Research Co. Inc., 22 Spencer, Stoneham, Mass 02180

[c]Lakeshore Cryotronics Inc., 9629 Sandrock Tr., Eden, N.Y. 14057

measurements. Since we anticipate growing highly compensated high-resistivity samples during this program, we constructed a third system which is capable of making Hall measurements on samples with resistances up to 10^{13} ohms.[a] A schematic of this apparatus is shown in Fig. 10.

3. Infrared Spectroscopy

The infrared transmittance spectra of GaP crystals were obtained with the Digilab FTS-14[b] Fourier Transform spectrometer. The samples were attached to the cold finger of an Air-Products[c] Cryo-Tip helium cryostat and cooled to about 8°K for measurement. The sample temperature was determined by using an Au-7 atomic percent Fe-versus-Cu thermocouple soldered to the cold finger. The sample surfaces were lapped and polished before measurement, with no chemical surface treatment being used. In most cases, the samples were lapped with a 1.0-degree taper in the thickness to eliminate interference fringes in the transmitted signal. The energy transmitted by the sample is measured and divided by the energy transmitted by the cryostat system without the sample. The sample and reference energy spectra are measured sequentially, so the transmittance is limited in accuracy by the stability of the spectrometer system and by the accuracy with which the cryostat can be repositioned between measurements. The reproducibility is generally better than 5 percent.

To obtain accurate measurements of the carrier concentration by infrared spectroscopic measurements, the absorption cross section of characteristic lines of impurity have to be determined. This is accomplished by first correlating the optical measurements with electrical determinations of carrier concentration on a few samples. Once this has been done, carrier concentrations can generally be determined to a precision of about ±50 percent.

---

[a] Dr. Patrick Hemenger of the Air Force Materials Laboratory assisted in the design of this system.

[b] Digilab Inc., 237 Putnam Ave., Cambridge, Mass. 02139

[c] Air Products and Chemicals, Inc., Allentown, Pa. 18103

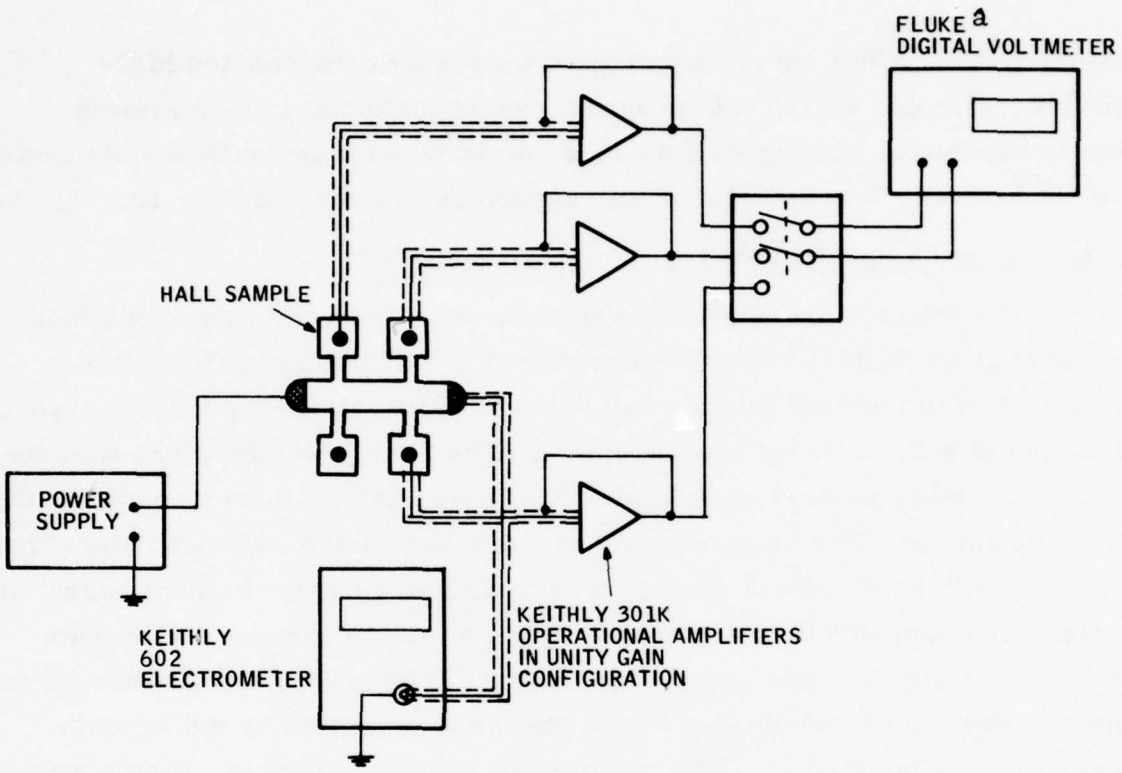

Figure 10. High-resistivity Hall apparatus schematic.

The photoconductivity system we have adapted for the FTS is shown schematically in Fig. 11. The sample is again cooled in the helium cryostat where the temperature can be varied from 300°K to about 5°K. The photocurrent is amplified and filtered with a PAR-114 signal conditioning amplifier used in conjunction with either the PAR-116 voltage preamplifier or the

---

[a]John Fluke Mfg. Co., Inc., P.O. Box 7428, Seattle, Wash. 98133

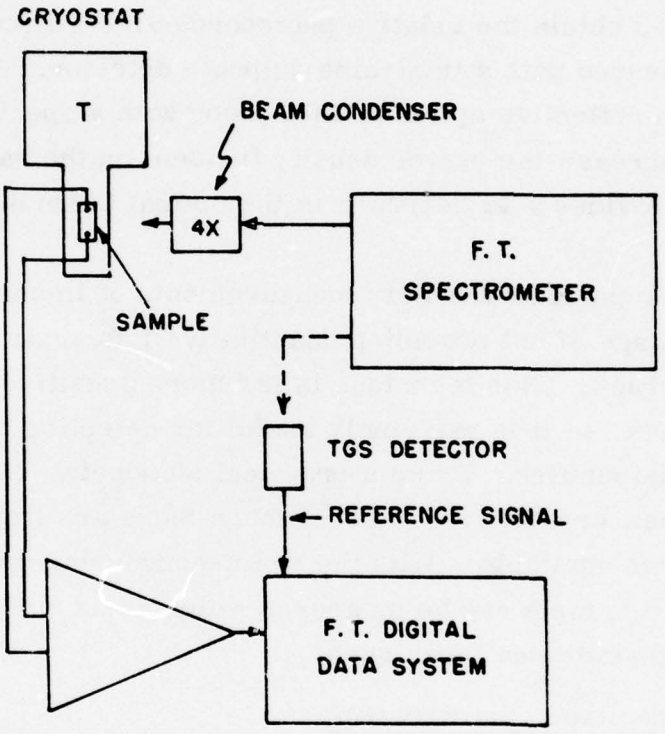

Figure 11. Photoconductivity system used with Digilab FTS-14 spectrometer.

PAR-184 current-sensitive preamplifier. The latter is used when the sample resistance becomes greater than about 10^6 ohms. The signal from these amplifiers is then further processed by the digital data system of the spectrometer. To obtain the relative photoconductive response, the energy spectrum is measured with a triglycine sulphate detector. A Harrick beam condenser[a] with reflective optics is used along with a specially modified cryostat system to increase the power density incident on the sample. The beam condenser provides a 4x decrease in the optical beam diameter at the focal point.

Extrinsic photoconductivity measurements of impurities generally have the disadvantage of not providing quantitative information on the concentration of the impurities. This technique is far more sensitive than the transmittance measurements, so it is extremely useful for detecting the presence of trace amounts of impurities. From a practical standpoint, this technique is also useful in a new crystal growth area where there are limitations on the size of the samples available. With the beam-condensing optics of the spectrometer, a small sample can be measured which could not be handled by the standard transmittance techniques.

4. Capacitance Spectroscopy

A schematic of the capacitance measuring apparatus is shown in Fig. 12. The lock-in amplifier is balanced with a standard low-loss capacitor in the circuit. The a-c measuring bias is supplied by the reference output of the lock-in. The unknown is then substituted for the standard, and a measurement of the in-phase and quadrature components of the current through the sample yield respectively the equivalent parallel capacitance and conductance of the unknown. The d-c sample bias can be varied from 0 to 250 volts. Measurements can be made over a frequency range from 100 to 2×10^5 Hz. The sample is mounted in a cryogenic dewar so the temperature can be varied from room temperature to 77°K. In addition, it is possible to illuminate the sample with two different radiation sources so it is possible to use this system for double-source photocapacitance measurements.

[a] Harrick Scientific Corp., Croton Dam Rd., P.O. Box 867, Ossining, N.Y. 10562.

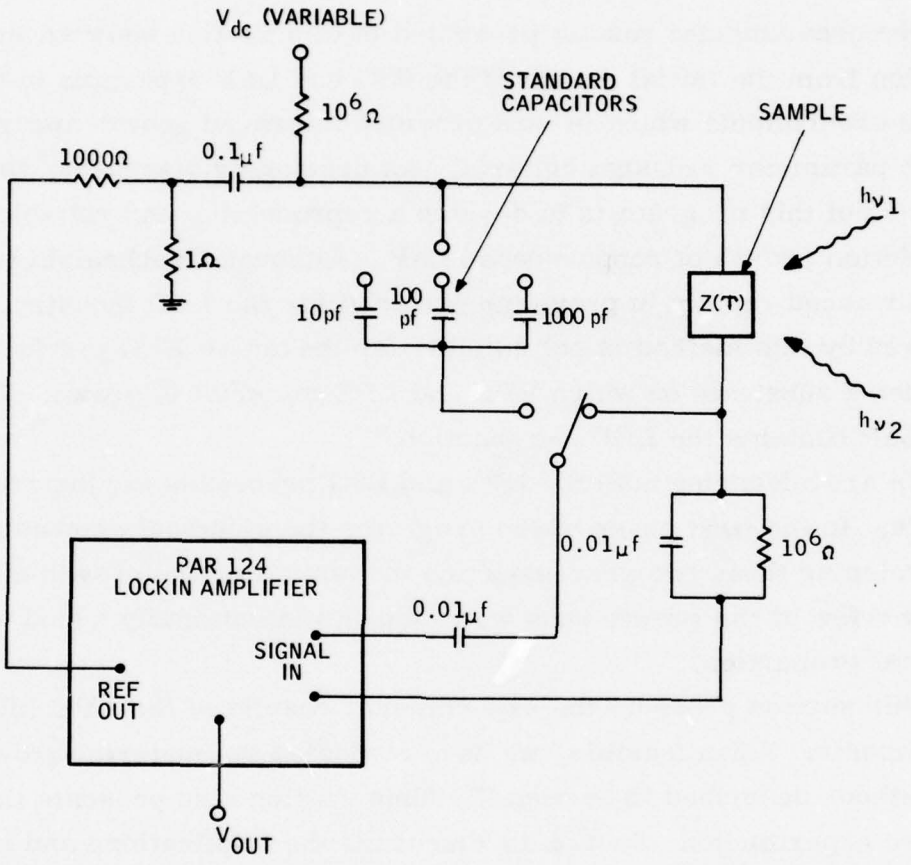

Figure 12. Capacitance-measuring apparatus schematic.

III. EXPERIMENTAL RESULTS

The experimental results presented in this section show an iterative progression from the initial design of the BSG and LPE apparatus to the first growth experiments which in turn provided improved growth apparatus and growth parameter redesign criteria. As previously discussed, the primary objective of this program is to develop a reproducible and reliable process for the solution growth of copper-doped GaP. Although Czochralski techniques have advanced rapidly in providing material for the LED industry, material prepared by this method is not suitable for the active LED p-n junction. It provides a substrate on which VPE and LPE material is grown. The VPE or LPE GaP contains the LED p-n junction.

We are advancing both the LPE and BSG processes for the growth of GaP:Cu. In the first phase of the program, the principal emphasis has been on developing these two processes and in controlling the growth morphology. In only a few of the growth runs were dopants intentionally added to alter the material properties.

This section presents the experimental results of the LPE and BSG growth experiments. When feasible, we have evaluated the material grown, using the methods described in Section II. This section also presents the results of these experiments. Section IV discusses the implications and conclusions which can be drawn from interpretation of these results.

A. Bulk Solution Growth

The 19 BSG runs made are outlined in Table 1. The first few growth runs were made to resolve some design details of the ampoule-crucible configuration necessary to prevent excessive vapor transport of GaP out of the crucible. BSG run 4 produced encouraging results. This growth run provided a void-free ingot of GaP which measured about 0.6 cm x 0.35 cm and which consisted of three or four single crystals. The ingot size was limited by the relatively short growth period (3.5 days) and its location in the tapered part (tip) of the crucible. Sections of this ingot are shown in Fig. 13.

TABLE 1. SUMMARY OF GaP BSG CRYSTAL GROWTH RUNS

Run Number	Time (days)	Starting Material	Crucible Temperature (°C)		Results
			Top	Bottom	
BSG-1A	---	Monsanto* polyporous chunk	---	---	Broken crucible
BSG-1B	6		963	888	No growth: excessive vapor transport out of unsealed crucible
BSG-2A	6.5		broken thermocouples		Sealed crucible in sealed tube; tube broken; small growth
BSG-2B	1.5		1000	870	Regrowth of unopened crucible from 2A; no outer tube; no growth
BSG-2C	4.5		1140	993	4mm-long polycrystalline growth
BSG-3	6		1118	914	No growth; insufficient starting material
BSG-4	3.5		1117	921	3mm-long growth, 3 or 4 single crystals
BSG-5	11.5		1117	920	No growth; excessive vapor transport of GaP to crucible plug
BSG-6	4		1099	883	Crucible shortened; vapor transport eliminated; 6mm-long polycrystalline growth
BSG-7	4.5		1050	924	6mm-long void-free polycrystalline growth; crucible loaded into hot furnace
BSG-8	5	GE** Czochralski, sulfur doped $\sim 10^{18}$ cm^{-3}	1058	920	11mm-long void-free polycrystalline growth
BSG-9	---		---	---	Furnace core burned out
BSG-10	11.5		1059	935	2cm-long single crystal
BSG-11	11	Same as BSG-8 and 4.8 mole % Cu	1063	907	Crucible expanded; polycrystalline growth filled with inclusions; first copper doping experiment
BSG-12	10	GE Czochralski, sulfur doped $\sim 10^{18}$ cm^{-3}	1060	935	First graphite crucible run; polycrystalline hollow-cone-shaped growth
BSG-13	9	IMANCO*** Czochralski and 6.0 mole % Cu	1059	935	8mm-long polycrystalline growth with some inclusions, plus 9mm-long polycrystalline growth with many inclusions
BSG-14	13	GE Czochralski, sulfur doped $\sim 10^{18}$ cm^{-3}	1059	790	Second graphite crucible run; air cooling of low-temperature end of growth tube; polycrystalline hollow-cone-shaped growth much like 12
BSG-15	10.5	Same as BSG-14 and 5.0 mole % Cu	1071	broken tc	Quartz crucible with air cooling of tip; growth started up from tip; aggregate of several small crystals
BSG-16	3	Same as BSG-14	1144	986	Quartz crucible-no furnance gradient forced air tip cooling (see Fig. 4); polycrystalline growth did not start at tip
BSG-17	12	Same as BSG-14	1140	995	Same arrangement as BSG-16 with increased tip cooling 1.5 cm long ingot increasingly single crystal toward top; convex growth interface
BSG-18	12.5	IMANCO Czochralski and 6.0 mole % Cu	1110	920	Quartz crucible-furnace gradient, no cooling; polycrystalline growth 2.5 cm long
BSG-19	11.5	Monsanto polyporous chunk	1135	1009	Same arrangement as BSG-17; ingot 1.6 cm long; increasingly single-crystal toward tip; convex growth interface

* Monsanto, Electronic Materials, P.O. Box 8, St. Peters, Missouri 63376

** General Electric Corp., Miniature Lamp Products Dept., Nela Park, Cleveland, Ohio 44112

*** IMANCO, 40 Robert Pitt Drive, Mansey, N.Y. 10952

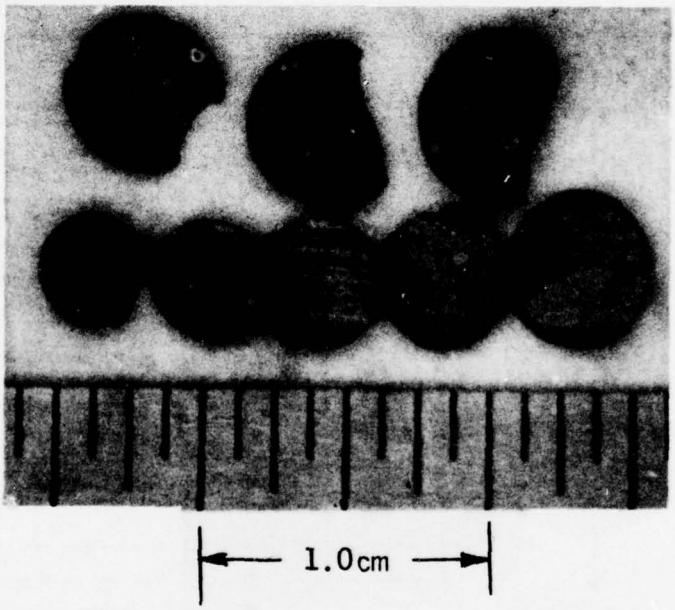

Figure 13. Sections of ingot from BSG-4.

In BSG run 6 the last vapor transport problem was eliminated by reducing the excess crucible volume above the melt and placing the top of the crucible at the highest temperature. The solid ingot grown in this run was even longer than BSG-4 but substantially more polycrystalline. BSG run 7 was loaded into the furnace after preheating to operating temperature. The purpose was to make certain that the crucible never experienced an inverted temperature gradient as might have occurred during heat up of the furnace. However the results of BSG-7, shown in Fig. 14, were much the same as BSG-6.

Runs BSG-8 through BSG-12 used sulfur-doped GaP starting material obtained from General Electric instead of the undoped polyporous Monsanto GaP. The identification of an acceptor in crystals from runs BSG-4, 6 and 7 led to this switch. BSG run 10 produced the large single crystals shown in Figs. 15 and 16. BSG run 11 was an attempt to duplicate 10, but with the addition of copper. The fact that the crucible expanded during growth indicates either poor evacuation at seal-off or accidental contamination with a volatile impurity.

The first run with the graphite crucible was BSG-12. Growth took place at the seed, but a solid ingot was not formed. Instead, growth occurred around the perimeter of the crucible, resulting in a hollow cone shape. Several crystals in the growth had dimensions of a few millimeters. The encouraging results were that the gallium did not wet the graphite, and, while the replaceable bottom end of the crucible had to be slit to remove the growth, the GaP did not adhere to the graphite the way it had to the quartz.

BSG-13 was the second growth run to which the copper dopant was added. GaP was grown over a 17-mm distance from the tip but was relatively polycrystalline with many Ga inclusions.

BSG-14 was the second growth run made with the graphite crucible. The bottom of the crucible had been machined and the bottom of the quartz tube flattened so as to increase the the thermal conductance between the growth charge and a cooling gas stream directed at the bottom of the tube. These modifications were not effective and the growth turned out much like BSG-12.

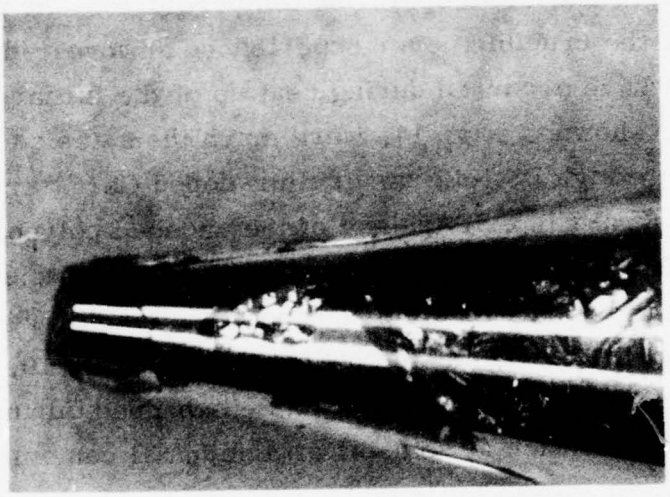

Figure 14. Ingot from BSG-7.

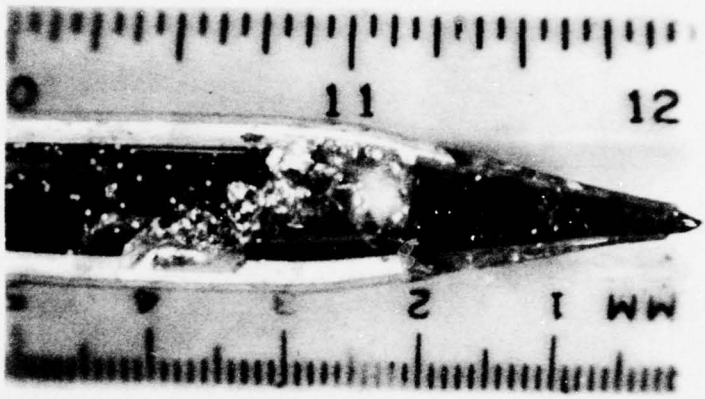

(a)

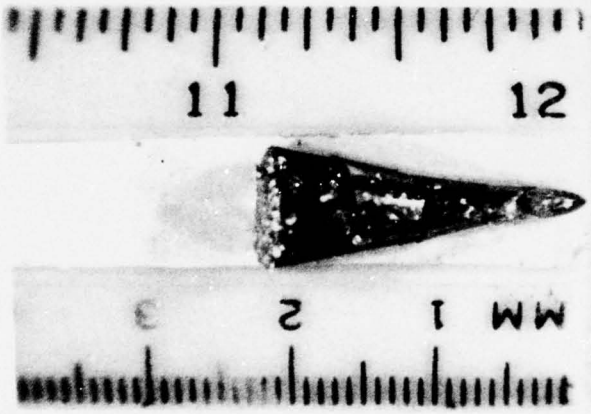

(b)

Figure 15. BSG growth (a) before and (b) after removal from quartz crucible; note in (a) that growth initiated at the tip.

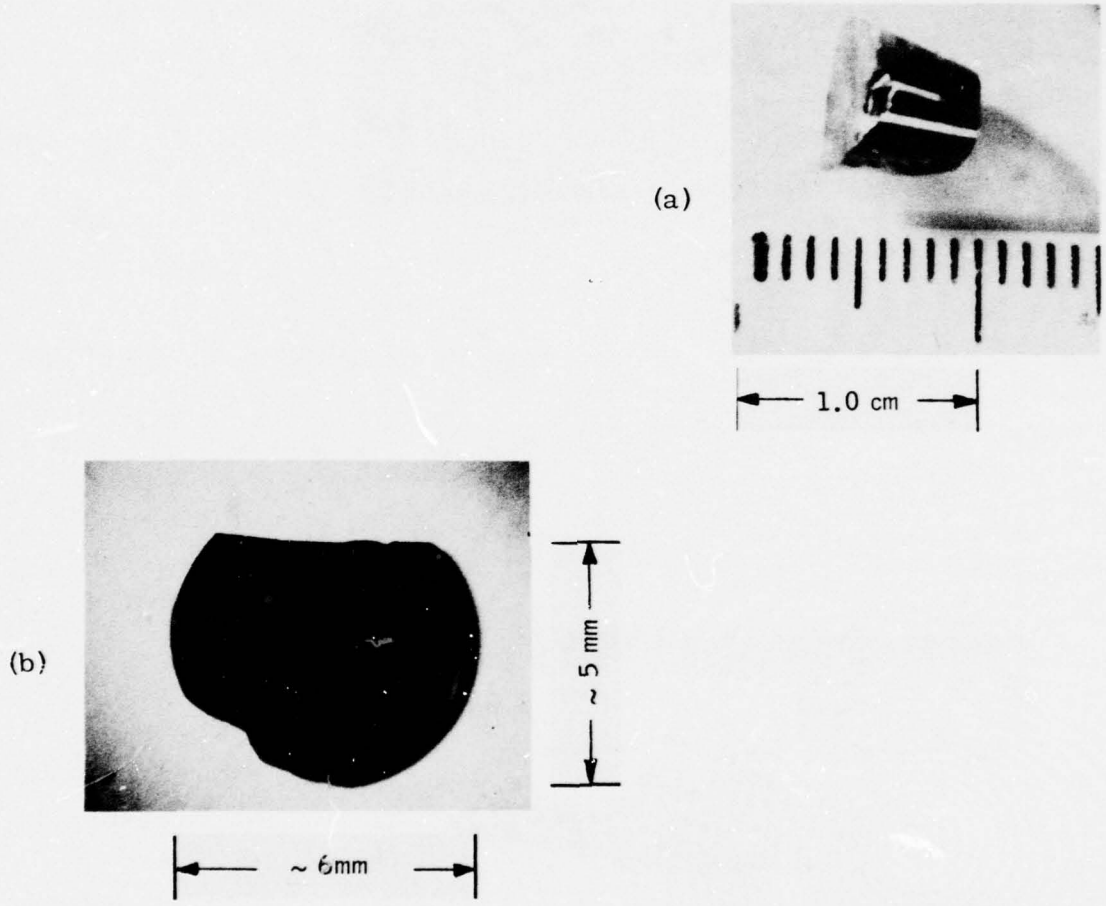

Figure 16. A GaP crystal (a) and GaP wafer (b) from BSG-10; note lack of grain boundaries and gallium inclusions.

A reconsideration of the crucible geometry for both the graphite and quartz crucible led to the conclusion that more drastic changes were required in the way in which the temperature gradient was established in the melt. Using a temperature gradient in the furnace tube to establish a gradient in the melt leads to the melt being hotter than the furnace ambient at the tip of the ampoule where growth takes place. This situation in turn results in a radial (outward) component of heat flow. Since the growth interface will follow the lowest temperature isotherm in the melt, it follows that a heat flow pattern that is longitudinally downward and radially outward will produce concave isotherms and hence a concave growth interface. We attempted to solve this problem by using an isothermal furnace environment combined with forced air cooling of a carefully restricted portion of the tip of the growth ampoule. Since these experiments were much easier to "cut and trim" with quartz than with the graphite crucible the latter was temporarily set aside. However, the graphite crucible with a seed crystal is definitely considered to be the most desirable approach.

BSG-15 was the first experiment using some of the ideas explained above. A temperature gradient in the furnace tube was still used, but in addition to forced air cooling of the tip. The cooling air flow was found to be inadequate and too much of the ampoule tip was exposed to the cooling flow. The shape and thickness of the quartz ampoule wall at the tip may also have contributed to crystal growth having started several millimeters up the wall instead of right at the tip.

BSG-16 was the first run using a flat furnace temperature profile and forced air cooling of the tip. The quartz skirt which restricts the cooling gas flow to a well defined area of the tip broke during the run resulting in an uncontrolled cooling pattern. A very polycrystalline ingot started at 10 mm from the tip and grew 12 mm long.

BSG-17 demonstrated that our decision to use a flat furnace profile and forced air cooling was correct. Crystal growth was initiated at the ampoule tip due to a thinner wall and more rounded shape and an ingot 1.5 cm long was grown as shown in Fig. 17. The most significant features, however, were the realization of a convex growth interface and the predicted increasingly single crystal nature of the ingot toward the top. A single crystal area 2 mm x 6 mm was found in a slice near the top of the ingot.

BSG-18 was started in another furnace tube before the results of BSG-17 were available. It was a Cu doped run using the furnace gradient arrangement without forced cooling. In contrast to BSG-17 the growth became more polycrystalline as it proceeded up the ampoule.

BSG-19 was essentially a repeat of BSG-17 except that (undoped) Monsanto polyporous chunk starting material was used instead of the 10^{18} cm^{-3} sulfur doped Czochralski GaP from G. E. As in BSG-17, an ingot was grown that was increasingly single crystal toward the top which again showed the convex growth interface.

B. Liquid Phase Epitaxial Growth

A series of copper-doped LPE common-source substrate growth runs was carried out at the beginning of the project to demonstrate, with a minimum of effort that GaP could be doped with copper via LPE. These experiments were successful in that compensated photosensitive GaP was grown; however, as expected, the grown surfaces were irregular with many growth steps and steep ridges at the edge. The technique was dropped in favor of the slider LPE technique. The slider shown in Fig. 6 was used for LPE runs 1 through 9. It produced layers 3 mm x 8 mm on slightly larger substrates. During the course of these runs several design improvements were incorporated in a new slider, previously described and shown in Fig. 7. This slider (No. 3) can grow larger areas (4.7 mm x 12.7 mm) and has a hole in the base for introducing cooling gas. Although the LPE growth cycle uses a cool-down to precipitate GaP from solution it is generally believed that it is necessary to maintain the substrate somewhat cooler than the melt to prevent dendritic growth which can result from constitutional super cooling. The LPE growth runs performed with slider 2 and slider 3 are listed in Table 2.

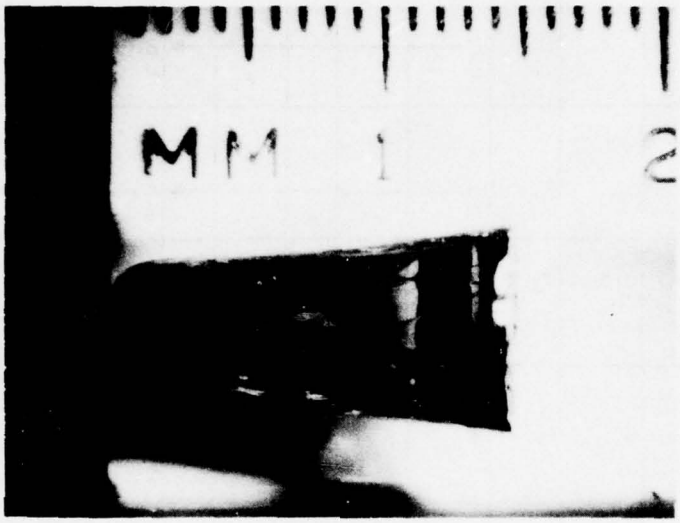

Figure 17. GaP crystal from growth run BSG-17.

TABLE 2. SUMMARY OF LPE GROWTH RUNS

Run Number	Growth Temperature (°C)			Substrate Orientation	Substrate No.	Mole % Cu	Atmosphere	Temp. Difference	Source GaP	Substrate GaP	Results
	Start	Stop									
LPE-1	1008	700	2°C/hr	<1/3° (1,1,1)	34 35 36 37	3.3 5.0 5.0 7.5	He	--	--	--	Slider stuck with growth columns over substrates layers thick but fairly smooth
LPE-2	97[illegible]	965		<2° (1,1,1)	38 39 40 41	0 0 0 0	He	--	--	--	Very good appearing layers; quite thin
LPE-3	1019	986			42 43	0 0	He	--	--	--	Wider temperature interval, layers correspondingly thicker
LPE-4	--	--			44 45 46 47	0 0 0 0	He	--	G.E.	G.E.	Vacuum leak; no growth
LPE-5	930	913			48 49	0 0	He	--			Layer somewhat off center of substrate; good appearance
LPE-6	975	963			50 51	0 0	He	--			Melt back; questionable film thickness
LPE-7	974	963			52 53	0 0	4%H_2 in He	--			Much cleaner growth charge after run; LPE layer thickness ~ 12 μm
LPE-8	975	951			54 55	0 0	4%H_2 in He				Similar to run 7
LPE-9	974	944			56 57 58 59	3.0	10%H_2 in He	--	A. D. Little	A. D. Little	Surfaces similar to two previous runs; growth steps and irregularities but specularly reflecting
LPE-10	964	20		<1.5° (1,1,1)	60 61 62 63 64 65	0 3.0 4.2 5.8 8.2 0	H_2	--	Monsanto IMANCO-2		First run with slider No. 3, substrates too thick; layers thin but quite smooth
LPE-11	1049	1044		<1.5° (1,1,1)	66 67 68 69 70	0 0 4.0 6.0 7.9	H_2	0.8°C	Monsanto	IMANCO-2 A. D. Little A. D. Little IMANCO-2 A. D. Little	Smoothest most uniform appearing layers to date

Four substrates were used in LPE run 1, with copper dopant concentrations spanning the likely range required for close compensation. The slider was moved to position the growth columns over the substrates at the starting temperature, but, after the growth cool-down, the slider could not be moved until the temperature was lowered all the way to 700°C. Nevertheless the LPE layers, one of which is shown in Fig. 18-a, appeared quite smooth. The undoped layers of LPE run 2 were much thinner as the short temperature growth interval would predict. LPE run 3, with a somewhat wider temperature growth interval, gave a correspondingly thicker layer. LPE run 5 used the lowest starting temperature of the series, but with no apparent effect on layer appearance.

The quantity of GaP starting material used in LPE run 6 was limited to less than that required to saturate the melt at the starting temperature. The additional GaP required to saturate the solution must, of course, come from the substrate. This run produced smooth surfaces, but there was serious doubt as to whether an LPE layer was formed at all.

LPE run 7 introduced the use of a 2% H_2 in an He reducing atmosphere. One of the layers, LPE 7-52, is shown in Fig. 18-b. The most obvious effect of the reducing atmosphere was to leave the surface of the growth charge very much cleaner than with 100% He. LPE run 8 doubled the percentage of hydrogen with the results similar to run 7.

LPE run 9 was the first copper doping run in a reducing atmosphere. The appearance of these layers was similar to previous runs which used the reducing atmosphere.

LPE-10 was the first run with the new slider 3. Both doped and undoped growth charges were prepared. Undoped source material, Monsanto Polyporous chunk, was used for the first time for all layers except LPE 10-65. With the new stainless steel safety tube encasing the alumina growth tube, 100% palladium diffused hydrogen was used as the growth ambient. The slider base cooling system was not operative during this run. The grown layers were found to be too thick to move the slider after the designed growth temperature cool down. Hence the substrates remained under the growth columns while

Reproduced from
best available copy.

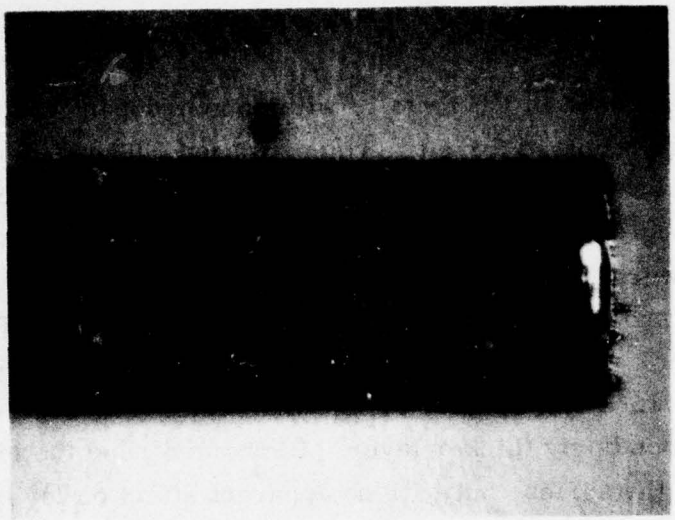

(a)

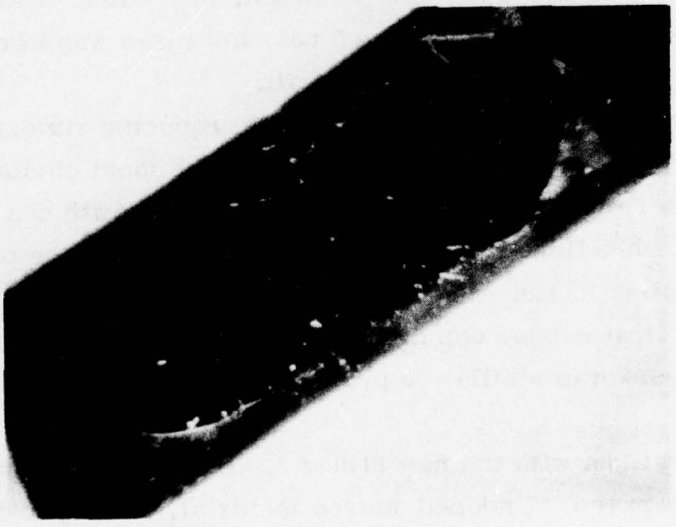

(b)

Figure 18. Layers from (a) LPE growth run 1 and (b) LPE growth run 7.

the furnace cooled to room temperature. The substrates were broken in the process of removing the slider, but the pieces were large enough to determine that the surface morphology was good. They were also large enough to provide samples for material evaluation.

For LPE-11 the substrates were lapped to give approximately 0.002 in. clearance after growth. The slider moved with ease and wiped all of the Ga from three of the five grown layers, and approximately 90% of the Ga from the remaining two layers. This growth run used the slider base cooling, with the flow rate such that the temperature drop in the base cooling hole was 0.8°C. The growth temperature interval was moved to a substantially higher temperature (1049°C) for this run (see Table 2). This temperature increase was based on increasing evidence, from both the BSG and LPE growth experiments, that close compensation of GaP is not achieved for temperatures less than 1000°C. In these experiments 4-8 mole % of copper was added to the growth charge.

This run produced the best LPE layers grown to date from the standpoint of surface morphology, and hence substantiates all of the design improvements which were incorporated into slider 3. Photographs of two of the five layers are shown in Figs. 19-a and 19-b. Large areas of the layers appear specularly reflecting to the unaided eye. Most of the texture seen in the LPE growth area is from the unpolished back surface of the substrate. Surface smoothness of one of these layers, LPE-66 was measured with a Tallysurf[a] instrument. The data are shown in Fig. 20. The line at A is the substrate base line for the left half of the figure and the line at C is the base line for the right half of the figure. The substrate and layer were broken at B and simply laid together for the measurement; hence the discontinuity at B. The most significant feature of this measurement is that over a length of 12 mm of LPE surface, the roughness exceeds 2 μm at only one point and is generally less than 1 μm. The

[a] Rank Precision Industries Inc., 411 E. Jarvis Ave., Des Plaines, Ill. 60018.

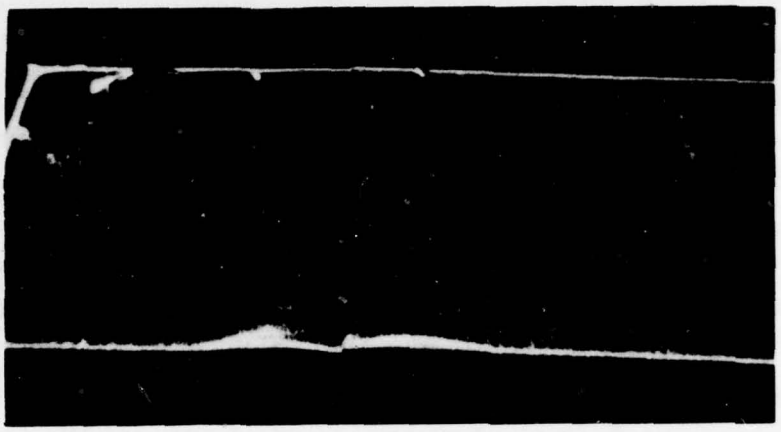

(a)

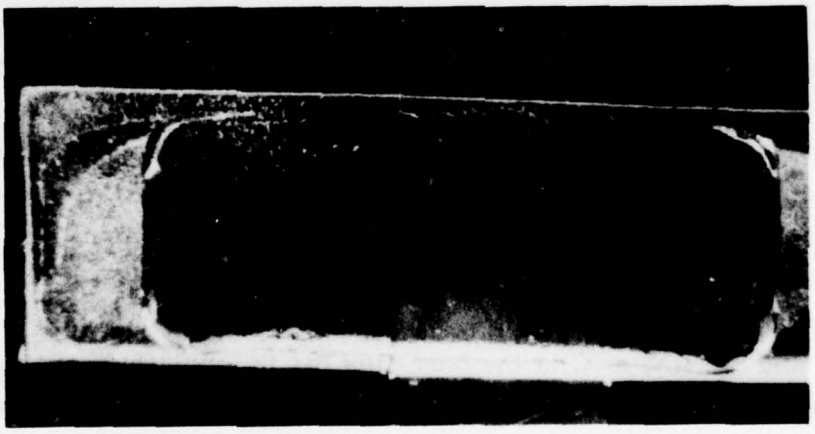

(b)

Figure 19. LPE layers from (a) LPE 11-68 and (b) LPE 11-70.

Reproduced from best available copy.

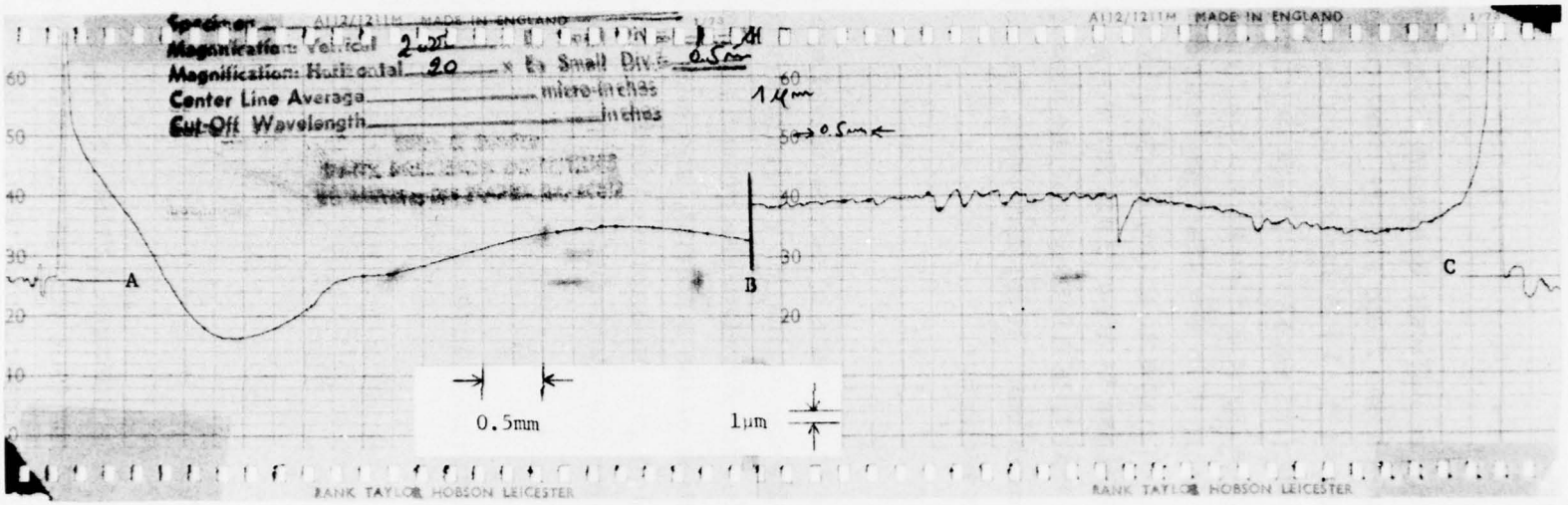

Figure 20. Surface smoothness measurement of LPE 11-66.

A. Substrate base line for left half of layer, A to B.

B. Discontinuity where substrate and layer are broken.

C. Substrate base line for right half of layer B to C.

uniformity in layer thickness is more difficult to assess from these data because the discontinuity at B prevents one from simply connecting the two substrate base lines A and C. Note that the LPE surface dips below the substrate surface between A and B, implying that some melt back occurred. If the ridge at edge A is ignored, then the layer thickness varies by approximately 4.5 μm along the 5.5 mm length from A to B. The layer thickness along the 6.5 mm length from B to C is much more uniform, varying by less than ±1.5 μm. The average layer thickness is about 5 μm for the segment from B to C. It should be pointed out that LPE 11-66 is not the smoothest or most uniform layer of the LPE-11 growth run. It is, however, the only one we have evaluated with this measurement technique.

C. Material Evaluation

This subsection summarizes the results of our material evaluation experiments. The objectives of the material evaluation program are twofold: (1) to characterize the material in order to correlate the growth parameters with the electrical and optical properties of the material, and hence to gain control over the material properties; (2) to gain an improved understanding of the basic mechanisms which determine the photoconductive and transport properties of GaP.

The material presented is discussed under the following subheadings:

- Photoconductivity
- Transport measurements
- Infrared absorption
- Capacitance spectroscopy

In previous publications[2][3] we have discussed these techniques and their application to the study of GaP. In the following paragraphs we present the principal results obtained during the present program. A discussion of these results is given in the next section.

1. Photoconductivity

The principal objective of the proposed program has been to achieve an improved understanding of the growth and material parameters which influence the phtotconductive properties of GaP:Cu; hence, an essential part of the material evaluation has been the measurement of the photoconductive effects in the material grown under this program. During the initial phase of this program, only a few of the growth runs were intentionally doped with copper (the sensitizing center in GaP), so our photoconductive experiments were not exhaustive. The photoconductivity experiments performed have, however, been very encouraging.

Our past experience with bulk solution growth has shown that as-grown GaP surfaces have a significantly lower surface recombination velocity than do lapped and polished surfaces. Consequently, for the LPE samples we are interested in the photoproperties of as-grown surfaces. Therefore the LPE samples for photoconductivity studies are not mechanically or chemically polished in any way. The only preparation prior to contacting is an organic solvent rinse followed by a series of deionized water rinses. The ohmic contact on n-type samples is made by evaporating 750Å of Ag:Te followed by 550Å of Ni and heat treating at 680° for 10 minutes. The BSG process, of course, does not yield as-grown surfaces. Samples grown by this technique are lapped flat and chemically-mechanically polished with a bromine-methonal etch before contacting. The ohmic contacting procedure is the same as for the LPE samples. For both types of samples the dark and photo I-V characteristic was linear for fields up to 10^4 V/cm. This indicates that the current transport in these samples is not limited by minority carrier sweep-out, space charge limited currents, or contact effects.

Early in the program a series of GaP:Cu LPE layers were grown (LPE 1-34 to LPE 1-37) to demonstrate the feasibility of growing GaP:Cu LPE layers using the slider technique. Figure 21 shows the relative spectral response of one of these copper-doped samples; note that the response extends out to about 3.8 eV. These samples were not optimally doped; the peak measured photoconductive gain on this sample was 23.

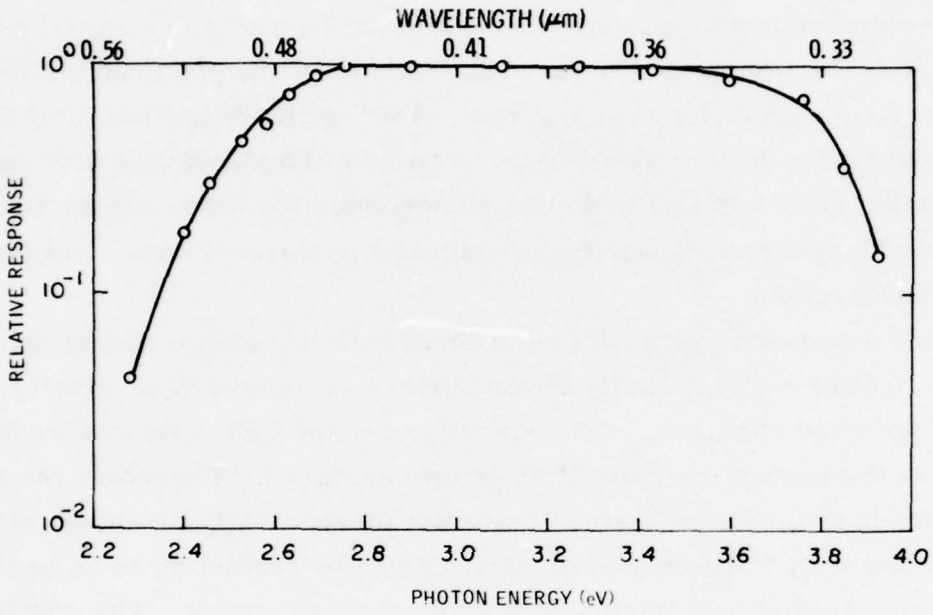

Figure 21. Relative spectral response as a function of photon energy for an LPE-grown GaP:Cu photoconductor.

Later in the program, after the LPE growth apparatus had been substantially improved by the design and construction of slider 3, additional experiments were conducted on the growth of GaP:Cu by LPE. These growth experiments are described above. The photoproperties of the samples from the last series of GaP:Cu LPE growth runs exhibited good photocharacteristics. The dependence of the photoconductive gain on incident photon energy for one of these samples is shown in Fig. 22. Note the soft edge near 2.2 eV, the peak at 2.7 eV and the relatively slow decline in photoconductive gain for photon energies above 2.8 eV.

The dependence of the photosignal on the incident flux intensity helps in identifying the photomechanisms. This dependence is also important from a device viewpoint. The photocurrent-radiation flux intensity characteristic for an LPE grown GaP:Cu photoconductor is shown in Fig. 23. Note that at the lower flux intensities the dependence is nearly linear and that at higher flux intensities the dependence becomes sublinear.

Another factor of considerable importance for a photoconductive device is the spatial uniformity of the detector response. Figure 24 shows the photosignal, as recorded on a storage oscilloscope, to a spot which is slowly scanned along the active area of one of the LPE-GaP:Cu samples which were grown early in the program. The length of the active area was 2.5 mm. Note that, over half of the active area, the response varies by less than 25 percent.

Figure 25 shows the spatial uniformity of three slits on one of the LPE GaP:Cu layers which was grown late in the program. Note the improvement in spatial uniformity over that of the earlier grown layer shown in Fig. 24. The dimensions of the active area for the samples in Fig. 25 were: slit 1, 0.2 cm x 0.002 cm; slit 2, 0.21 cm x 0.007 cm; slit 3, 0.08 x 0.002 cm. All of these data were taken with a 0.01-cm-diameter spot of 2.7 eV radiation with an intensity of 5×10^{15} photons/cm^2-sec.

While the LPE GaP:Cu samples discussed above were Cu doped and hence sensitized they were not closely compensated. The sample resistance was < 1000 ohms. Hence, all of the above measurements were taken in the a-c

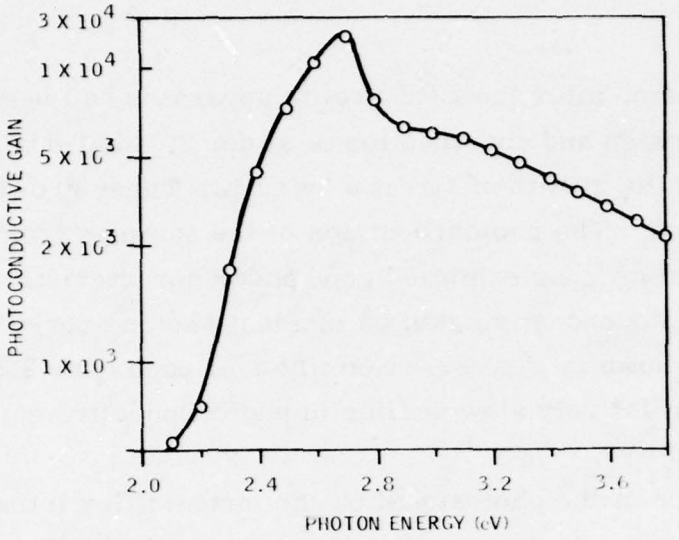

Figure 22. Photoconductive gain versus photon energy for LPE 11-69 GaP:Cu photoconductor.

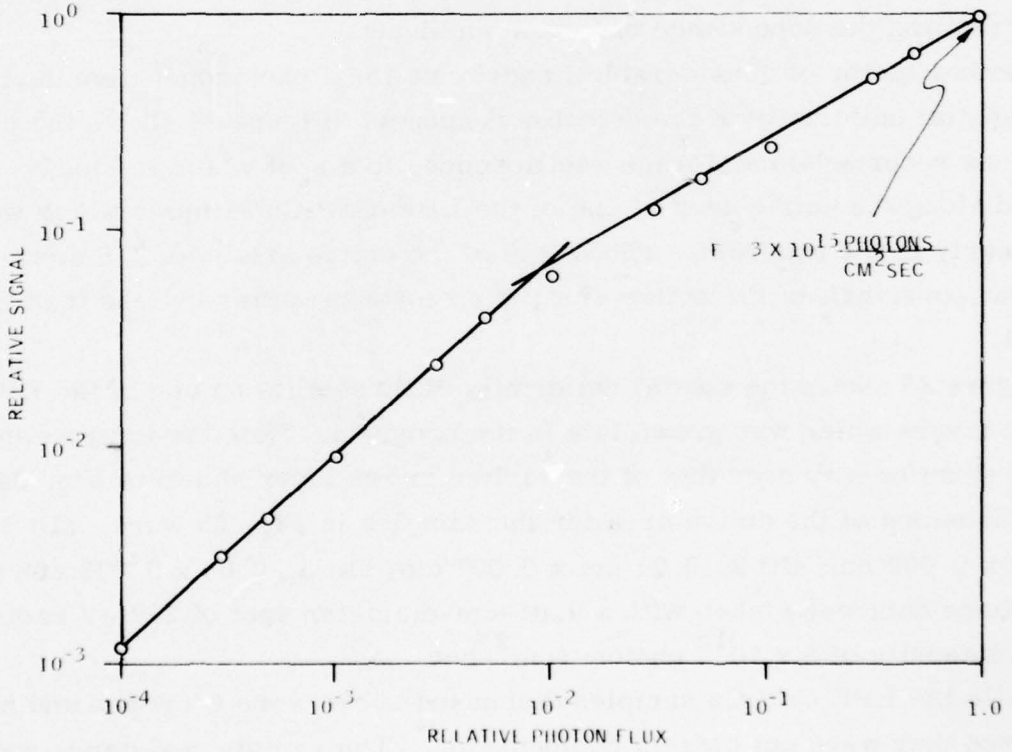

Figure 23. Photocurrent versus radiation flux intensity at 2.7 eV for LPE 11-69 GaP:Cu photoconductor.

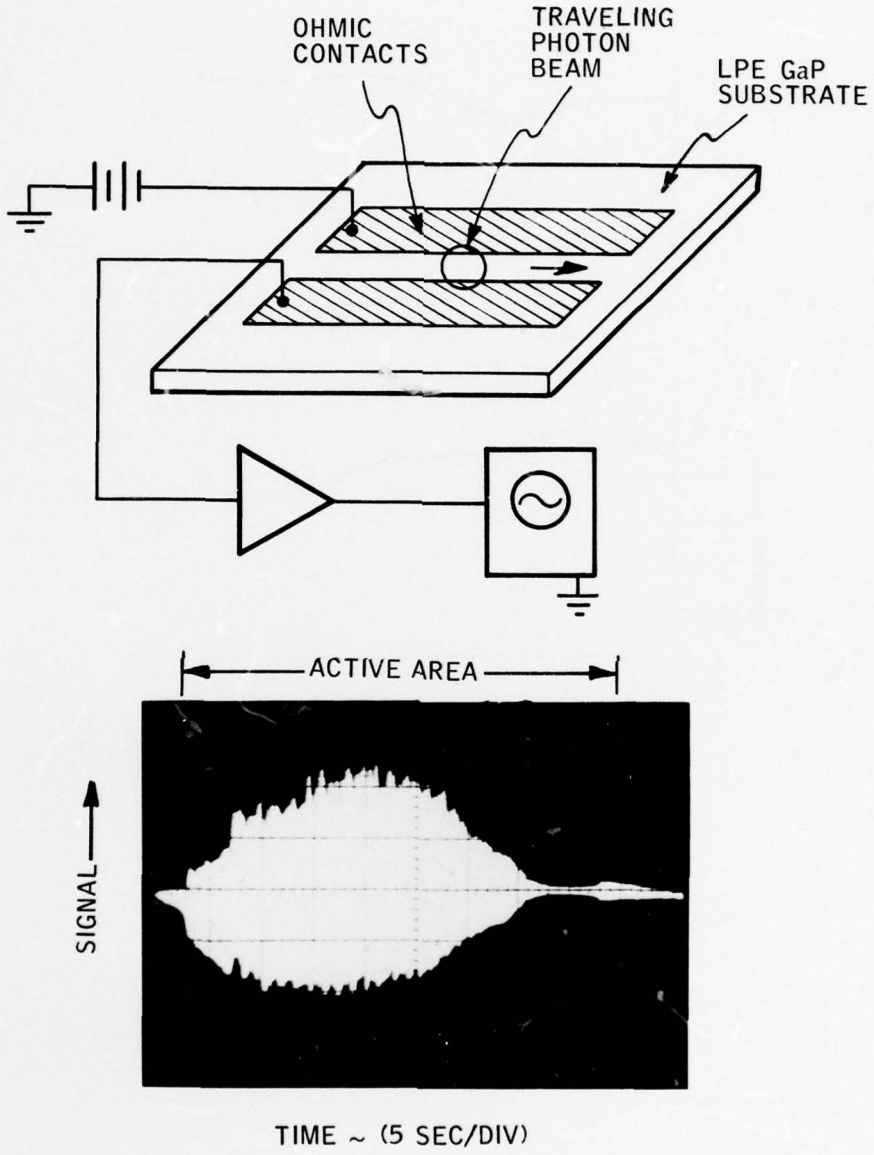

Figure 24. Photoresponse of a GaP:Cu photoconductor to a slowly traveling photon beam.

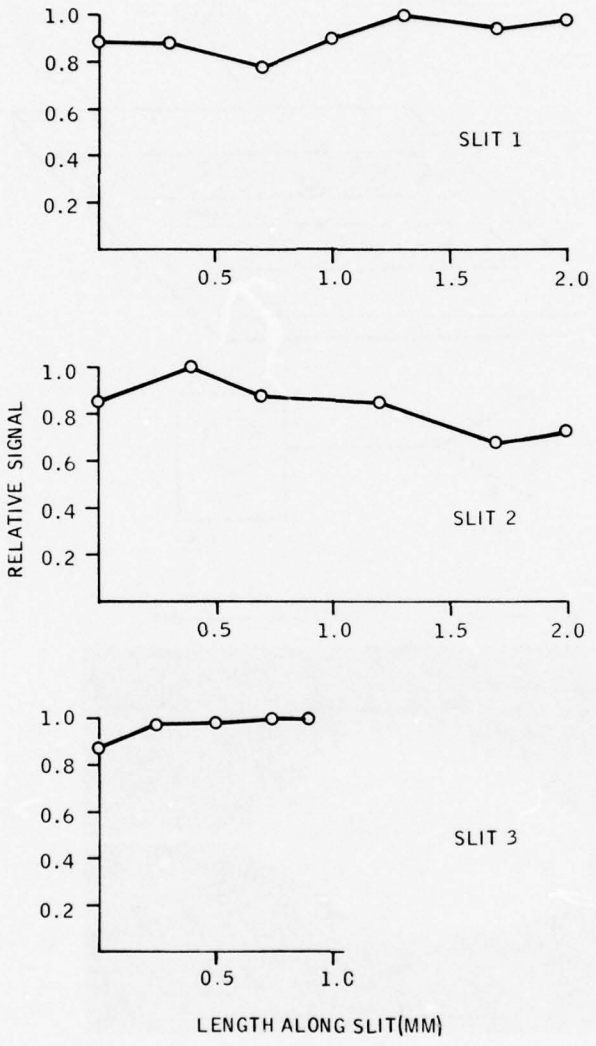

Figure 25. Spatial uniformity of three photoconductors from LPE 11-69 GaP:Cu.

mode at a low frequency (~ 15 Hz). A typical frequency response for one of the LPE GaP:Cu photoconductors is shown in Fig. 26. Note that at high frequencies the response is asymptotic to the response curve for a single time constant of 4×10^{-4} sec. In space navigation systems the radiation detectors must be capable of operation at 30 Hz.

As discussed in Section II, most of the BSG growth runs were performed to establish and study the growth parameters. We did, however, look at the spectral response of samples from undoped (i.e., no intentional dopants added to the growth charge) growth runs; a typical result is shown in Fig. 27. The shape of this response curve is as expected for a sample fabricated on an interior surface. Note the decline in the spectral sensitivity above 2.8 eV. An intentionally copper-doped sample on an interior surface will exhibit a similar spectral response, but with photoconductive gains of 10^2 to 10^4.

2. Transport Measurements

Hall and resistivity analyses were routinely made on samples from each BSG growth run which yielded material which was amenable to this type of analysis. Most of the LPE layers were grown on heavily doped low-resistivity substrates, and hence it was not possible to perform Hall analysis on these samples. However, a few LPE layers were grown on highly compensated Czochralski substrates and measurements were made on one of these layers. All of the Hall and resistivity data were taken using the van der Pauw technique. The samples were lapped flat and chemically polished in a hot potassium ferricyanide etch [0.5 M KOH, 1.0 M $K_3Fe(CN)_6$]. For n-type samples ohmic contacts were achieved by alloying from small peripherial In:Te dots at 680°C. For p-type samples In:Zn dots were alloyed at 420°C to form the ohmic contacts.

The material parameters which are generally available from Hall analysis are majority carrier type and concentration, majority carrier activation energy, and the temperature dependence of the resistivity and majority carrier mobility. The first three of these parameters were of the most interest to us in evaluating the material from these early growth runs. Table 3 tabulates these parameters for each of the growth runs on which data were taken.

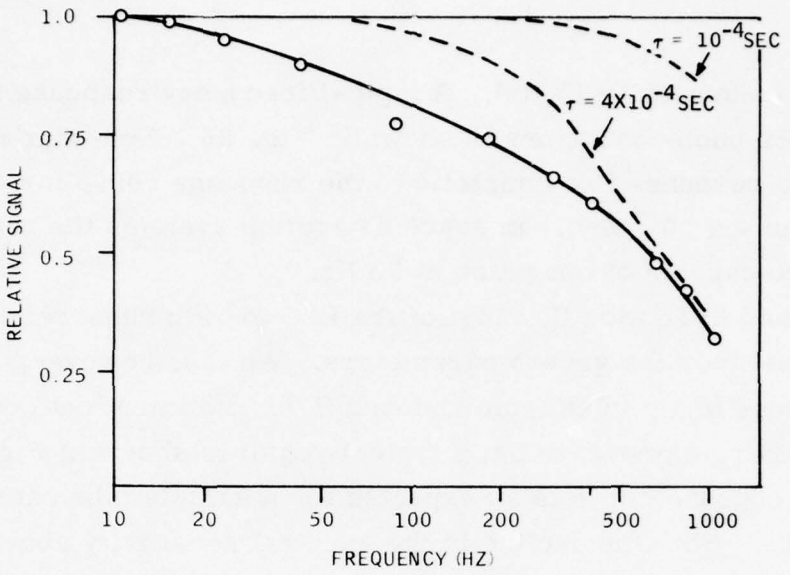

Figure 26. Frequency response of photoconductor from LPE 11-69 GaP:Cu (the dotted line represents the frequency dependence for a single time constant).

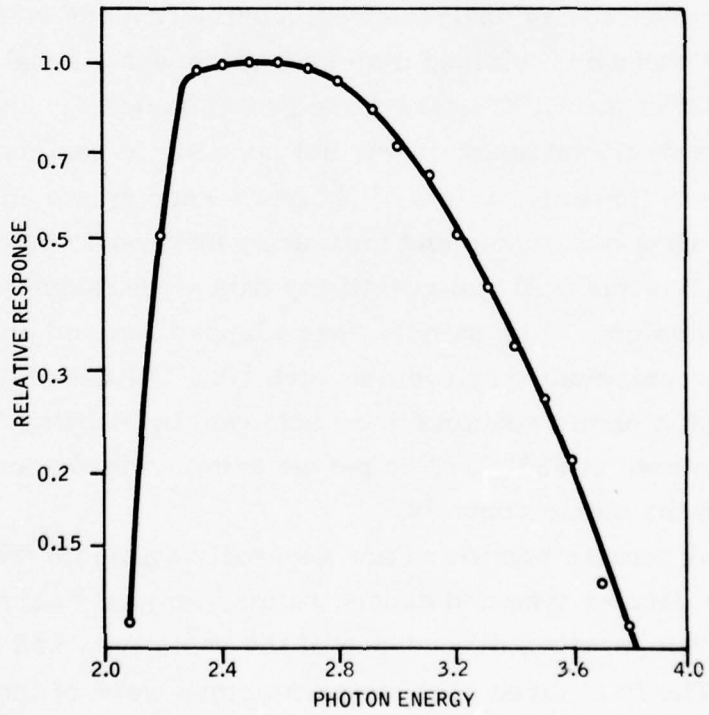

Figure 27. Relative photoresponse as a function of photon energy for a lapped and polished BSG-10 surface.

TABLE 3. TABULATION OF HALL DATA

Growth Run Number	Carrier Type	Room-Temperature Carrier Concentration (cm^{-3})	Principal Donor/Acceptor Activation Energy (eV)
1	Insufficient material for analysis	---	---
2	Polycrystalline material	---	---
3	No growth occurred	---	---
4	p	1×10^{17}	< 0.060
5	Insufficient material for analysis	---	---
6	p	$\sim 1.2 \times 10^{10}$	---
7	p	5×10^{16}	0.042
8	n	7×10^{17}	0.095
9	No growth occurred	---	---
10	n	3×10^{17}	0.093
11	Insufficient material	---	---
12	Polycrystalline material	---	---
13	p	9×10^{15}	< 0.060
14	Polycrystalline material	---	---
15	n	8×10^{17}	0.090
16	n	2.9×10^{18}	0.097
17	n	2.1×10^{17}	0.089
LPE 63	n	6.8×10^{17}	0.095

The first BSG growth runs which used Monsanto polyporous chunk starting material were p-type. Figure 28 is a plot of the carrier concentration divided by $T^{3/2}$ versus reciprocal temperature for a representative Hall sample from one of these p-type growth runs. These particular variables are plotted because the straight-line segment of this curve (which is the carrier freeze-out region) gives the carrier activation energy. For this particular sample, the acceptor activation energy is 0.042 eV. The same measurement

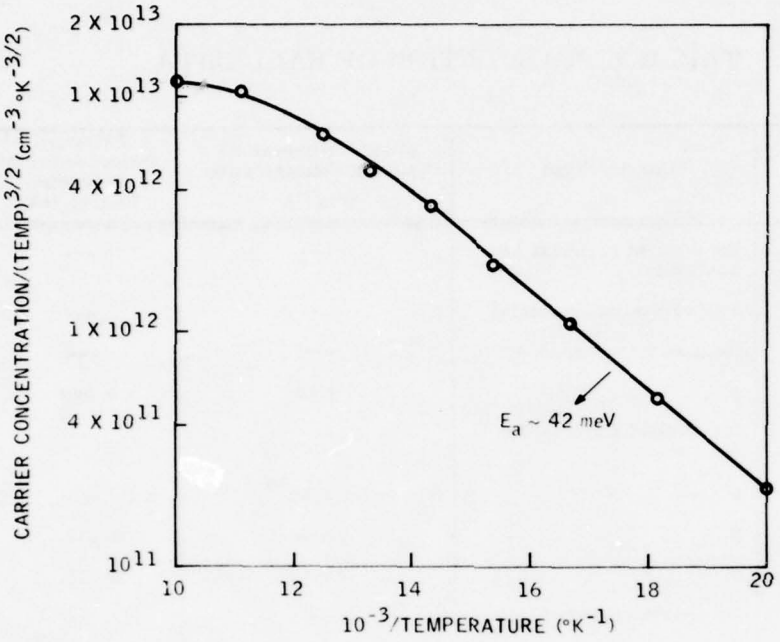

Figure 28. Carrier concentration divided by (temperature)$^{3/2}$ as a function of reciprocal temperature for BSG-7.

yields a room-temperature p-type carrier concentration of 5×10^{16} cm^{-3}. Oscillatory photoconductivity measurements (discussed below) on similar material yield an activation energy of 0.050 eV. We now believe that this low-energy acceptor state in GaP is due to carbon. A positive determination of the source of this carbon in the growth process has not been made. The principal reason for developing the BSG growth technique was to obtain larger, more uniform GaP crystals than were obtainable from the random nucleation solution growth process. Hall data from growth run BSG-10, which, as discussed earlier, produced large single crystals, demonstrates the uniformity of the BSG material. Two Hall samples, spaced about 0.3 cm apart, were cut from a single wafer. The carrier concentration over $T^{3/2}$ versus $10^3/T$ is plotted in Fig. 29 for each of these samples. The carrier concentrations at each temperature for these two samples are within experimental error of being equal to each other.

In each of the Hall runs the temperature dependence of the mobility was measured. Figures 30 and 31 are plots of the mobility as a function of temperature for two n-type BSG samples. On Fig. 30 straight lines for a $T^{-1/2}$ and $T^{-3/2}$ temperature dependence are also drawn. The temperature dependence of the Hall mobility for a typical BSG p-type sample is plotted in Fig. 32 along with straight lines showing a T^{-3} and $T^{-1.5}$ temperature dependence. Figure 33 shows the temperature dependence of the mobility for an LPE n-type layer. Note that the low-temperature mobility is rather low. This LPE layer was grown from a copper-doped melt. In previous experiments with GaP:Cu we observed that as the copper concentration in the melt increased the mobility decreased. Note that, near room temperature, the mobility for this sample also varies as $T^{-3/2}$.

3. Infrared Spectroscopy

It is well established that optical absorption is a useful technique for investigating impurities in Si and Ge, and we have used this technique to evaluate the material grown on this program.

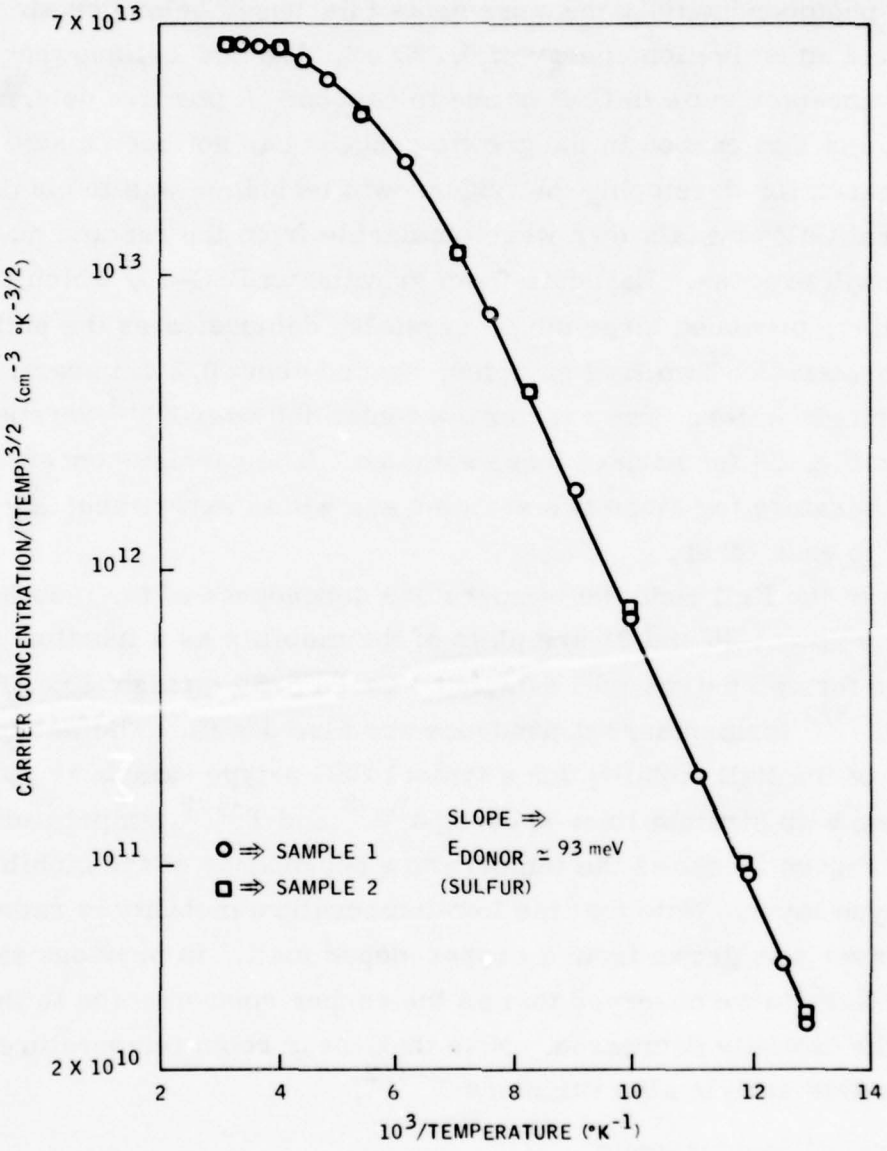

Figure 29. Carrier concentration divided by (temperature)$^{3/2}$ for two samples from BSG-10.

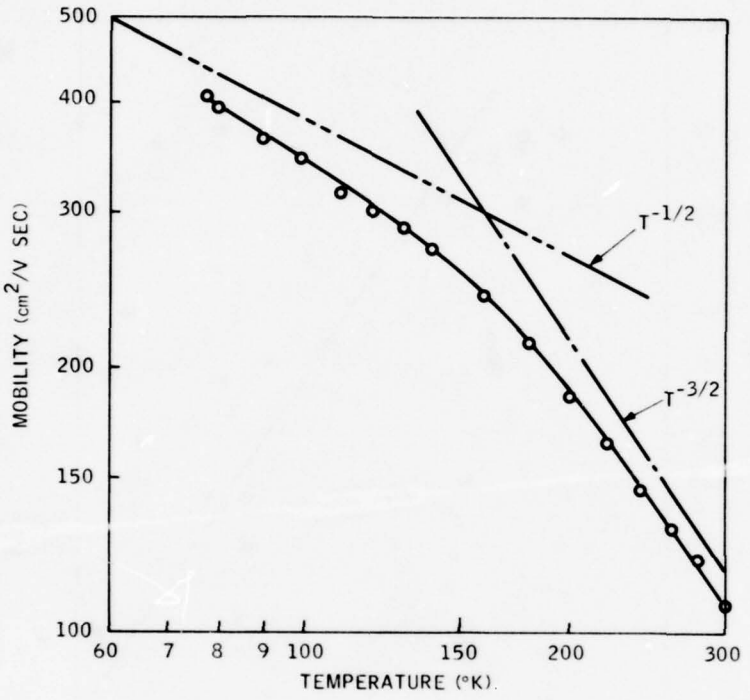

Figure 30. Temperature dependence of the mobility for an n-type sample from BSG-10 ($n = 3 \times 10^{17}$ cm^{-3}).

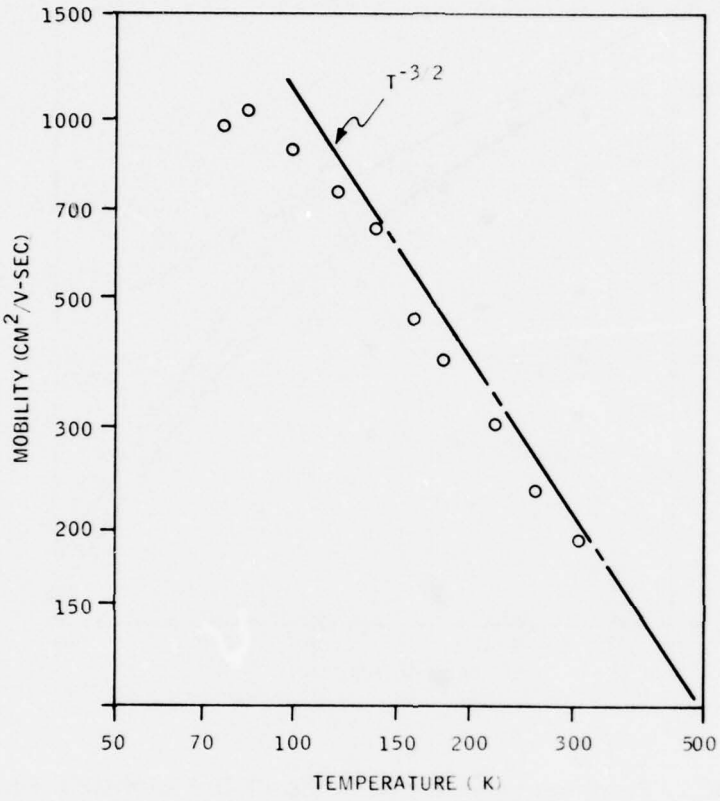

Figure 31. Temperature dependence of the mobility for an n-type sample from BSG-15 ($n = 8 \times 10^{17}$ cm^{-3}).

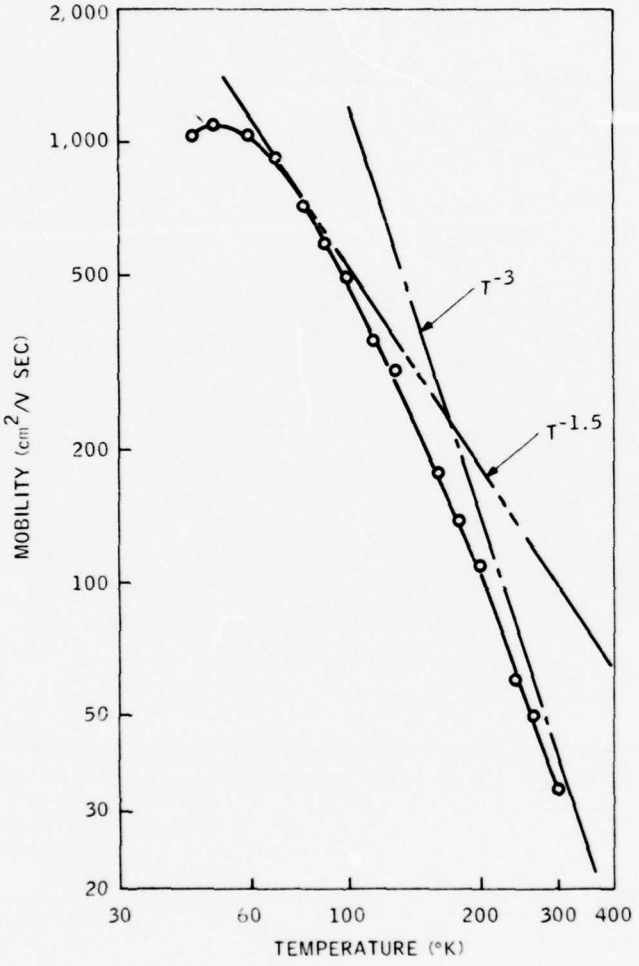

Figure 32. Temperature dependence of the mobility for a p-type sample from BSG-10.

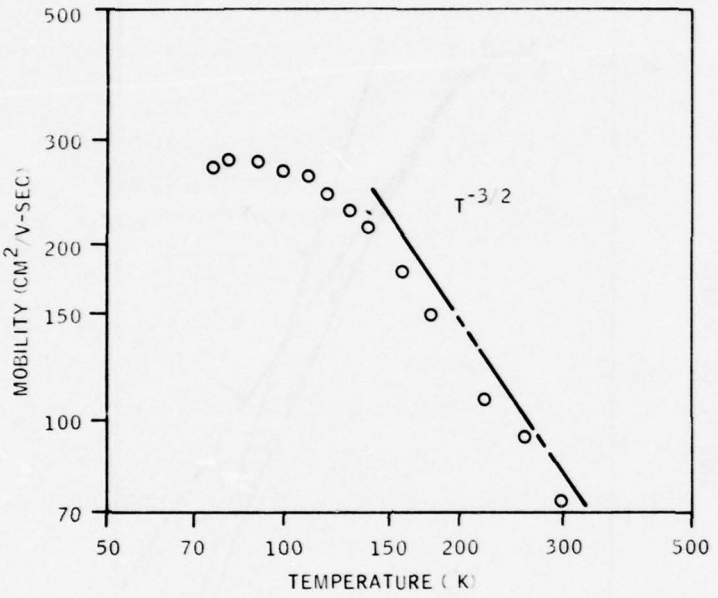

Figure 33. Temperature dependence of the mobility for a LPE 10-62 n-type sample.

The three shallow donors, S, Si, and Te, appear to be the ones most commonly occurring in GaP. In fact, S and Si probably are the most important since these two are often inadvertently introduced by the growth processes. These impurities have ionization energies between about 80 and 100 meV, so they have absorption lines in the mid-infrared part of the spectrum.

The low-temperature, infrared-absorbance spectrum of GaP doped with both S and Si is shown in Fig. 34. In this case, the absorption coefficient is shown as a function of the photon energy, expressed in wave numbers. The structure around 600 cm^{-1} and 800 cm^{-1} has been identified as being due to electronic transitions at S and Si impurities. The transitions due to these impurities have been marked "1" through "5" for the S lines, "a" and "b" for the Si lines. The small absorption bump at about 850 cm^{-1} is due to the S impurities being ionized, but the corresponding absorption edge due to the ionization of Si at about 660 cm^{-1} is not obvious in the absorption curve as shown in Fig. 34. The remaining absorption lines not specifically identified in Fig. 34 are due to two-phonon absorption processes in GaP. The presence of phonon absorption lines in this region makes it difficult to pick out all the impurity lines. To better observe the impurity absorption lines, difference absorption measurements were usually made. This was done by first measuring the low-temperature absorbance in a Zn-doped (p-type) sample, then subtracting this from the absorbance in n-type samples. Subtracting this absorbance from the spectra in n-type samples will leave only the effects of the impurities. With this technique, the detection limit for sulfur or silicon was about $1 \times 10^{15}/cm^3$.

The results of our initial studies indicate that we have a feasible means of measuring the electrically active S and Si concentrations in GaP by measuring the optical absorbance of the crystal cooled to liquid He temperatures. Unlike electrical measurements, which yield only the total electrically active donor concentration, optical measurements can determine the various species present as well as their concentration. This was demonstrated on a number of different samples where both the S and Si concentrations could be determined from the optical measurements.

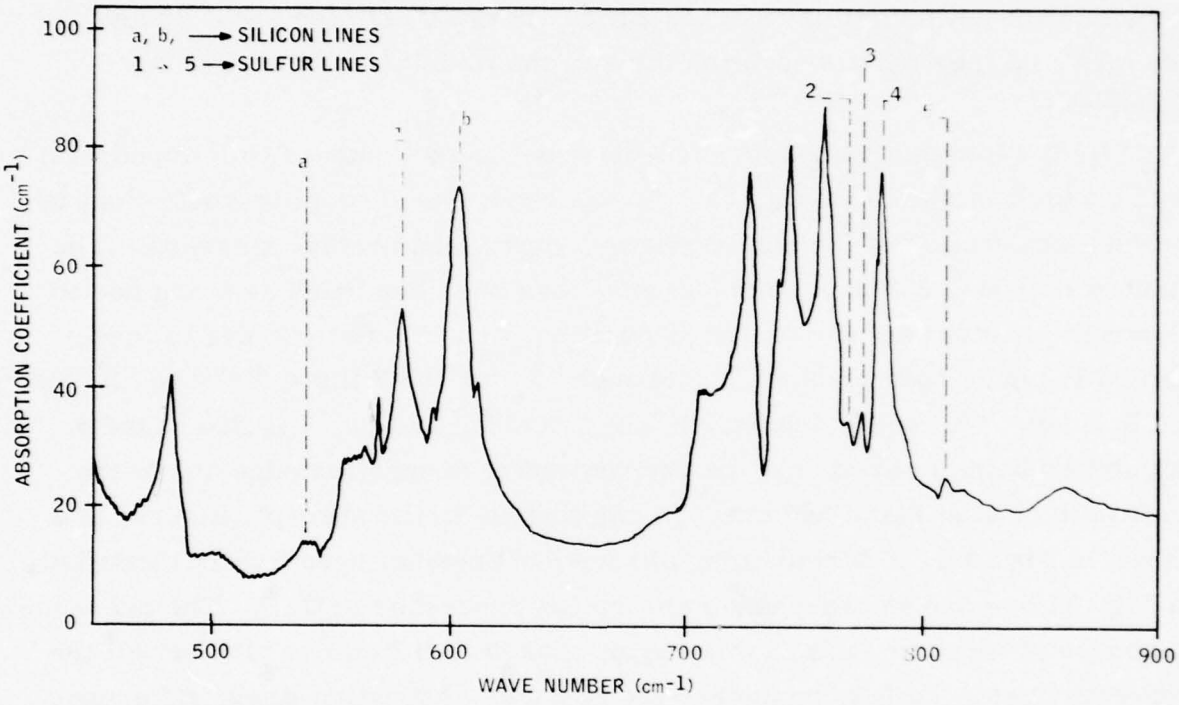

Figure 34. Absorption spectrum as a function of wave number for GaP containing S and Si.

The crystals investigated, and the impurities which we have identified by infrared techniques, are summarized in Table 4. The GE crystal, which was purchased from General Electric to be used as starting material for the growth experiments, was found to contain about $7 \times 10^{17}/cm^3$ sulfur impurities. The crystals grown from this material were found to also contain sulfur, but at a lower concentration. In the case of crystal BSG-11, the sulfur concentration is substantially lower than in the GE crystal because of the copper added to the starting Ga solution.

Carbon has been identified in all the material grown by the BSG process. The method of detecting carbon by absorption is illustrated in Fig. 35. This is a portion of the absorption spectrum of crystal BSG-10 taken with the sample at both 82°K and at 5°K. In the center of the figure, the strong absorption line is due to the $1s \rightarrow 2p_o$ transition in sulfur (line 1 in Fig. 33). As can be seen, the intensity of this line increases dramatically when the sample is cooled from 82°K to 5°K. In fact, this line was totally absorbing at 5°K because of the thickness of the sample used in this measurement. Similarly, the sulfur lines between 700 cm^{-1} and 800 cm^{-1} were totally absorbing. Nevertheless, the presence of the strong absorption at 577 cm^{-1} clearly identified sulfur as the dominant shallow donor in this crystal. The fact that its intensity did not change with temperature indicates that it is a lattice local mode vibrational line due to carbon on the phosphorus sites. Since the crystal is n-type, these impurities are compensated. The concentration of carbon is estimated to be about $1 \times 10^{17}/cm^3$ in this crystal.[4]

Carbon has also been identified in crystal BSG-4 by photoconductivity measurements. The relative photoconductive response in the 400 to 4000 cm^{-1} region of crystal BSG-4 is shown in Fig. 36. From Hall measurements this crystal was determined to be p-type with a carrier concentration of about $3 \times 10^{17}/cm^3$. Note that there is response down to the reststrahlen band which extends from about 300 to 400 cm^{-1}. Since the lattice will be totally absorbing in the reststrahlen band, it is impossible to determine if the extrinsic edge lies within this region. Also, it should be noted that the photoconductive response is oscillatory in nature with a period of about 400 cm^{-1}. The

TABLE 4. SUMMARY OF IMPURITIES FOUND IN GaP

Crystal	Type	Impurities	Concentration (cm^{-3})	Method	Starting Material
General Electric (GE)	n	S	7×10^{17}	Absorbance	
BSG-4	p	C Si	- - -	Photoconductivity	Monsanto
BSG-8	n	C	$\sim 2.5 \times 10^{16}$	Absorbance	GE
BSG-10	n	C	$\sim 1 \times 10^{17}$	Absorbance	GE
		S	$> 2 \times 10^{17}$		
BSG-11	n	C	$\sim 5 \times 10^{16}$	Absorbance	GE
		S	2.5×10^{17}		(4.8 mole % Cu)
BSG-12	n	C	$\sim 1 \times 10^{17}$	Absorbance	GE
		S	$> 3 \times 10^{17}$		

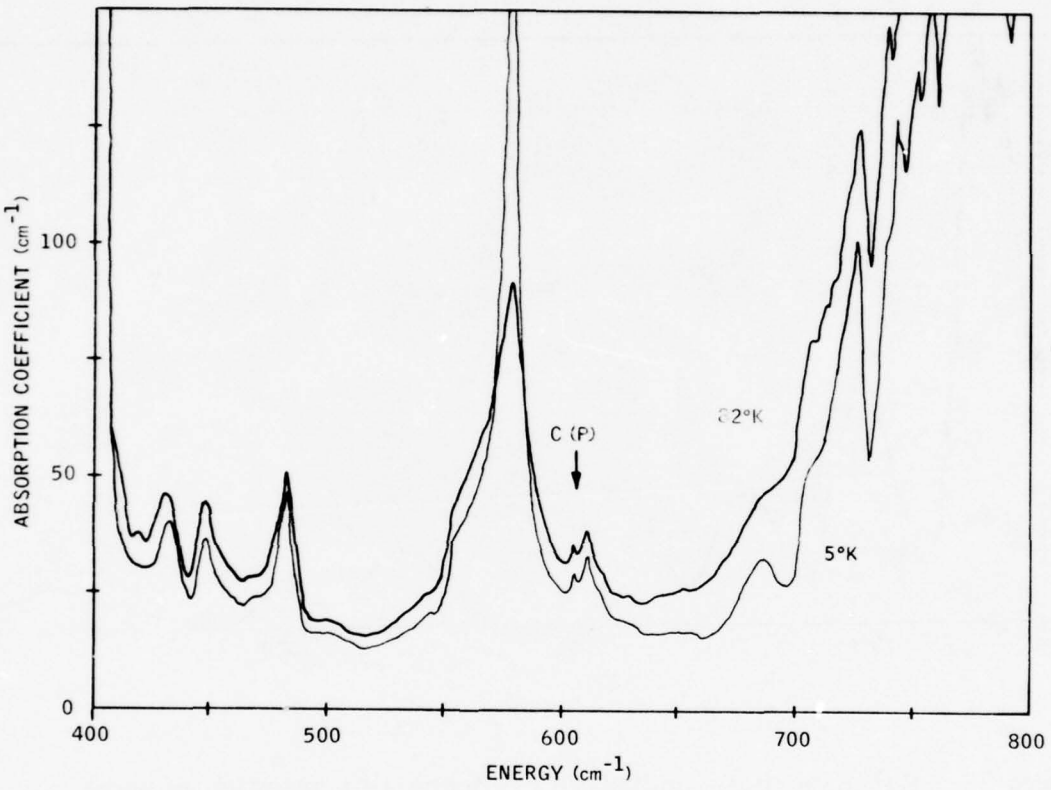

Figure 35. Absorption coefficient as a function of wave number for BSG-10 at 82°K and 5°K.

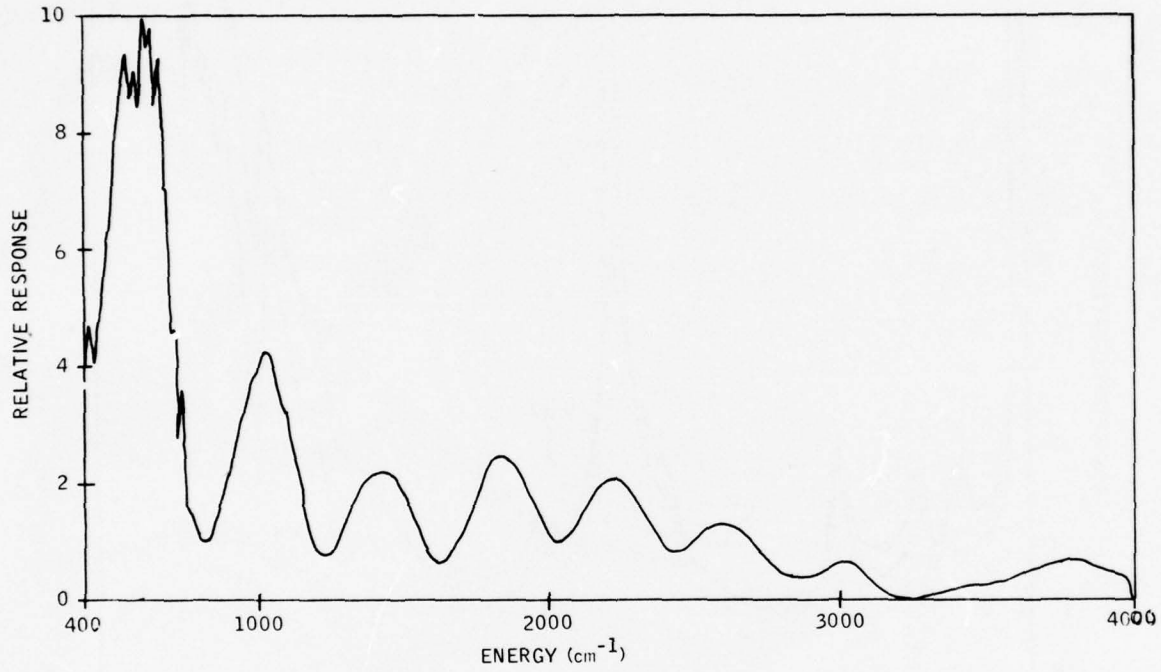

Figure 36. Relative photoconductive response as a function of wave number for BSG-4 at 7°K showing the oscillatory behavior of the photoconductivity.

sharp structure in the 400 to 1000 cm^{-1} spectral region is not noise, but is due to lattice absorption. The oscillations are "damped out" at about 3000 cm^{-1}, but additional structure is observed at higher energies indicating the presence of deeper impurity levels, possibly silicon acceptors. The interpretation of these data is given in Section IV-C.

4. Junction Capacitance Studies

We have routinely used the C-V characteristics of a Schottky diode to measure the impurity profile in the GaP LPE layers. Figure 37 shows a typical $1/C^2$-versus-V plot at room temperature for a Schottky barrier formed on a GaP substrate. Due to a peculiar set of growth conditions described above, one of the series of copper doped LPE runs was grown from 964°C to room temperature. This resulted in a thick (~ 100 μm) LPE layer. The first 50 μm of the layer was angle lapped and a row of Schottky barriers were fabricated on the lapped and as-grown surface. The voltage intercept obtained by extrapolating the linear region of the C^{-2}-V characteristic to zero gives the diffusion potential for a Schottky diode. The results of the C-V measurements for three of these diodes is shown in Fig. 38. These data show that the carrier concentration decreases with distance from the surface. Note that the extrapolated voltage intercept for each of these C^{-2}-V plots is near 1.2 eV which is approximately the diffusion potential in sulfur doped GaP.

Two capacitive techniques were used to investigate deep levels in GaP. The first technique, which is termed "Admittance Spectroscopy of Impurity Levels in Schottky Barriers," has been recently described by D. L. Losee.[5] In this technique a small a-c voltage is applied to a Schottky barrier diode. As the bias voltage is changed the quasi-Fermi level is swept through the various defect levels. As the Fermi level crosses the defect level, charge carriers are freed; this in turn alters the charge distribution within the depletion layer. The differential capacitance is determined by the magnitude of the charge oscillation, $\delta\rho$, per voltage amplitude, δV. So long as the frequency of voltage oscillation is sufficiently low and the temperature sufficiently high

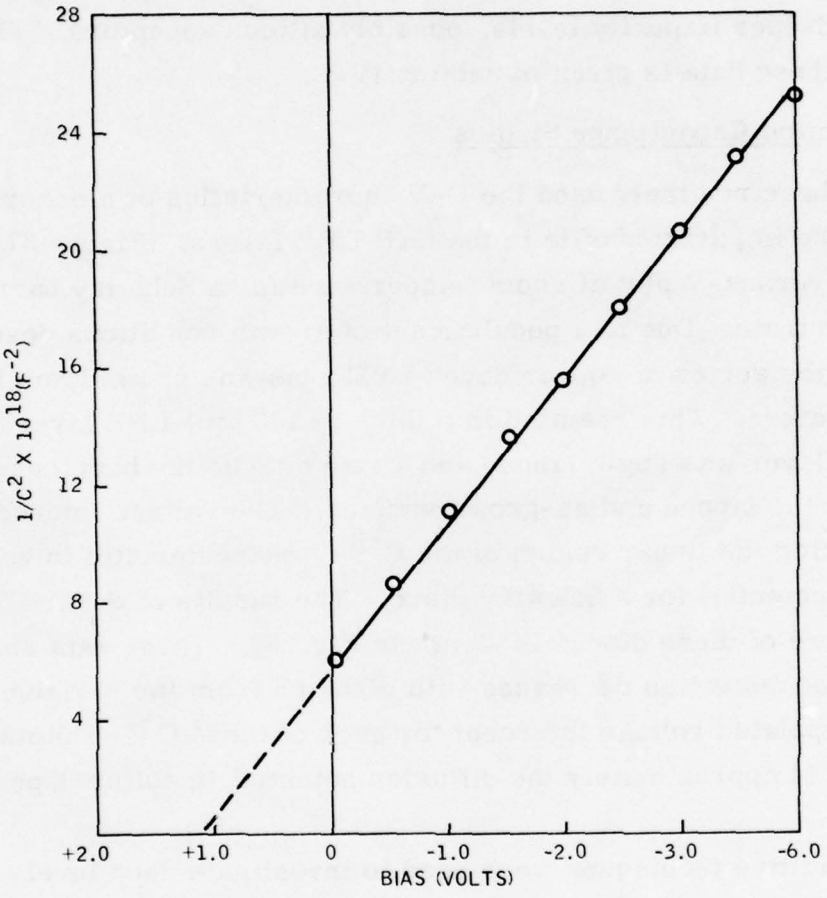

Figure 37. Reciprocal capacitance squared as a function of potential for a reverse-biased Schottky barrier.

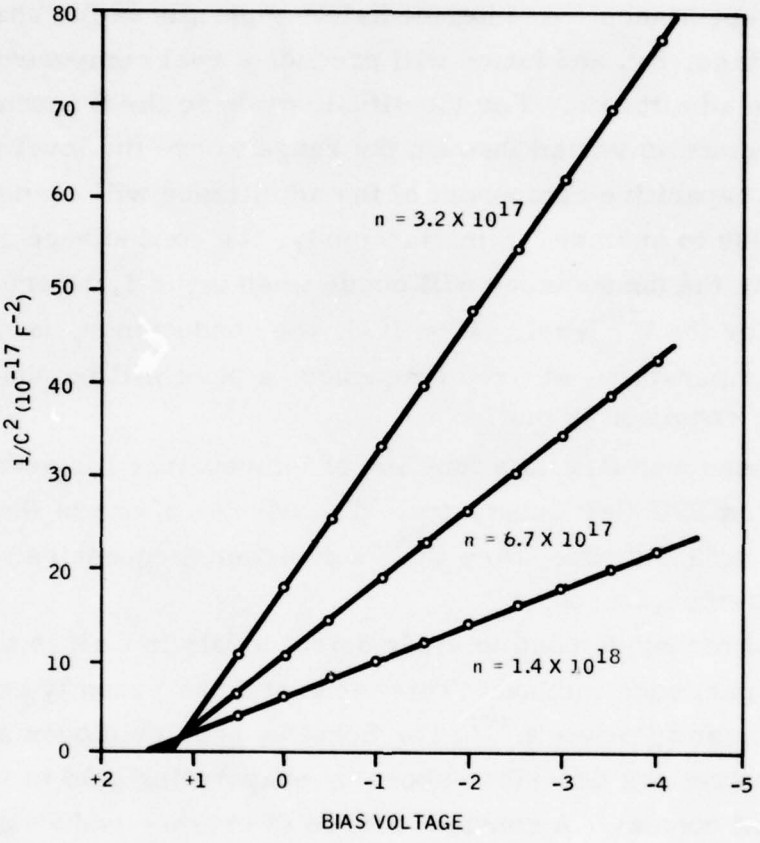

Figure 38. Reciprocal capacitance squared as a function of potential for three reverse bias Schottky barriers on an angle lapped LPE 10-63 surface.

so that the charge can move in and out of the level, the level will contribute to the capacitance. However, when either the frequency of the applied bias or the temperature changes so that the level cannot respond there will be a change in the capacitance. At intermediate temperatures the charge, $\delta\rho$, will lag the voltage, δV, and hence will produce a real component (i.e., conductance) to the admittance. For the situation where the frequency is fixed and the temperature is varied through the range where the level makes the transition, the capacitive component of the admittance will change monotonically from one value to another. Simultaneously, the conductance goes through a peak. A peak in the conductance will occur when $\omega\tau_k = 1$, where τ_k is the time constant for the k^{th} level. Thus if G, the conductance, is measured as a function of temperature, at fixed frequency, a peak will be observed each time an $\omega\tau_k = 1$ condition is met.

We have measured G/ω as a function of temperature for several Schottky diodes formed on BSG GaP substrates. The results of one of these experiments are shown in Fig. 39. Note that, for higher frequencies, the peak occurs at higher temperatures.

The second technique used to study defect levels in GaP is the double-source photocapacitance method. This technique has recently been discussed by White, Dean, and Porteous.[6] The Schottky barrier diodes are fabricated on the GaP substrate as described above by evaporating gold to form a thin semitransparent contact. A constant source of priming radiation of energy greater than the bandgap energy is maintained on the sample. A second, variable energy source (the probing radiation) is simultaneously directed on the sample, and the diode capacitance is measured as the energy of this source is varied. The steady level of priming radiation serves to create a steady-state population of electrons on traps above the Fermi level and of holes on traps below the Fermi level. Above the appropriate photon energy thresholds, the probe radiation upsets these populations by transfer of carriers to the nearest band edge. In the depletion region, these carriers are swept away by the field, and the charge distribution is altered with a corresponding change in the capacitance. The capacitance can be increased or decreased depending on the nature of the trap.

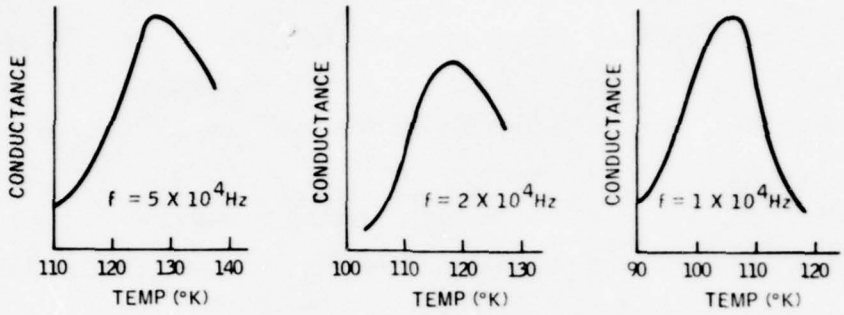

Figure 39. Conductance as a function of temperature at three different frequencies for a GaP/Au Schottky barrier on a BSG substrate.

Figure 40 shows the result of our measurement of change in capacitance of Schottky barriers formed on a BSG substrate as a function of the probing radiation energy for three different measuring frequencies. The dependence of the photocapacitance on the energy of the probing radiation can give information about the defect levels. Figure 41 shows the results of a similar measurement for a Schottky diode formed on an LPE substrate. Figure 41 also shows that in the absence of the primary radiation the capacitive effect of the probing radiation is absent.

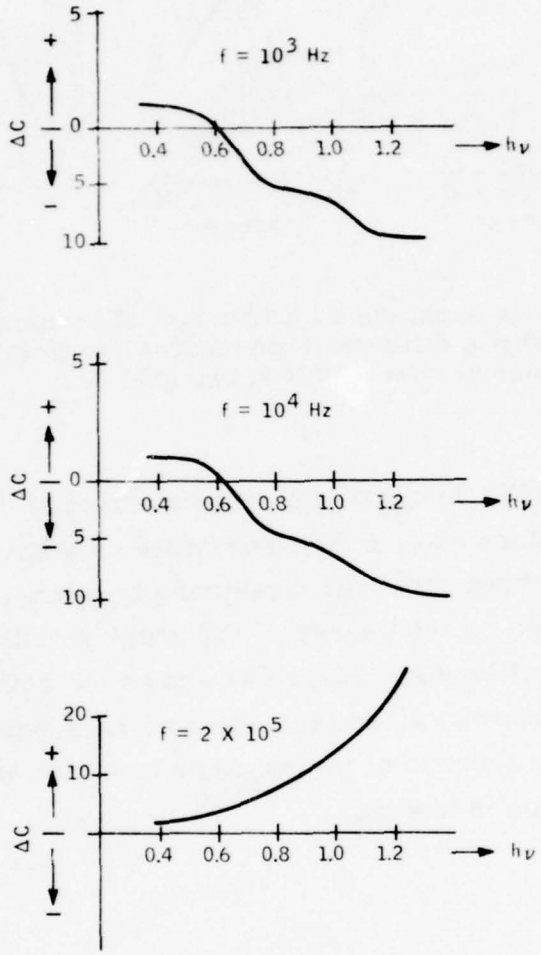

Figure 40. Dependence of the capacitance on the energy of the probe radiation at three frequencies in a GaP/Au Schottky barrier (the sample is simultaneously illuminated with 2.8 eV radiation).

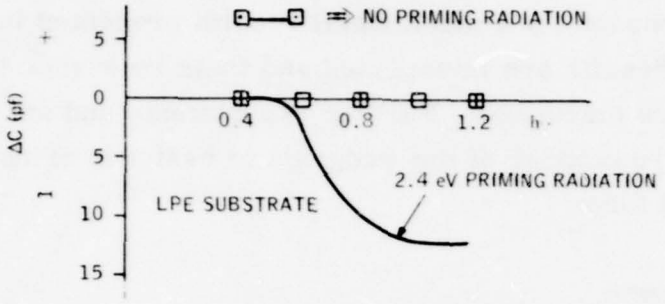

Figure 41. Dependence of the capacitance on the energy of the probe radiation for an LPE GaP/Au Schottky barrier.

IV. DISCUSSION

This section discusses the experimental results presented in Section III. Where possible, the results are interpreted and their relevance to the program at its present point are discussed. Further experiments and analysis will be conducted during the remainder of the program to assist in bringing our conclusions to their final form.

A. Bulk Solution Growth

The liquid-solid interface which occurs during solidification from a melt (whether or not it is stoichiometric) will, in general, be perpendicular to the direction of heat flow. The ideal liquid-solid interface shape for the BSG system would be slightly convex. This shape promotes the growth of a single crystal for the reason that, since growth proceeds perpendicular to the interface, any crystal grain boundary that exists at the interface will be carried, as the crystals grow, toward the nearest point on the crucible wall where it will be terminated.

In trying to establish the maximum temperature gradient in the Ga-GaP solution, one would prefer to have a steep gradient in the furnace along the length of the crucible. However, the Ga metal is a relatively good thermal conductor which is terminated on the cool end by a much poorer thermal conductor (the quartz tube). This results in the Ga-GaP solution at the cool end of the crucible being somewhat hotter than the furnace environment directly alongside of the crucible. Heat flow thus acquires a radial component outward as well as a longitudinal component. The results, in terms of crystal growth, range from a tendency to form polycrystal rather than single-crystal ingot, to the growth of a hollow-cone-shaped, very polycrystalline mass.

We believe this analysis accounts for the crystal growth morphology seen in BSG runs up to BSG-17. The heat flow pattern was somewhat more ideal with the single sealed quartz crucible runs than with the graphite crucible runs, both of which produced hollow-cone-shaped very polycrystalline growths.

The results of BSG-17 verify our analysis of the crystal growth dynamics. By generating the temperature gradient in the gallium solution with forced cooling of the crucible tip while using a flat furnace profile, the temperature in the gallium solution near the bottom of the crucible will actually be higher than the furnace tube temperature. Any radial component of heat flow will therefore be inward and when combined with the downward longitudinal component of heat flow will produce convex isotherms. The growth interface was convex in both BSG-17 and BSG-19. This result in successive growth runs confirms our analysis. The increasingly single-crystal nature of the ingots from these two runs demonstrates that we have the correct basic BSG design to achieve substantial improvement in single-crystal size.

We still believe that the graphite crucible is preferable to quartz. Ample evidence exists in the scientific literature that solution growth in quartz containers leads to silicon and oxygen contamination. A graphitie crucible is easily configured to use a seed crystal. We believe the use of a seed crystal is an important asset in minimizing polycrystalline growth from the very start of growth and therefore maximizing the single-crystal volume of the ingot. Graphite also eliminates the bonding of the GaP to the crucible wall.

Our graphite crucible and quartz ampoule are presently being redesigned to operate in a flat furnace temperature profile with forced air cooling. The task is to make the thermal conductance of the end of the graphite crucible and its quartz ampoule as high as possible. With a graphite crucible and GaP seed crystal properly operating in a flat furnace profile and with the gradient generated by forced-air cooling we believe we will achieve the desired BSG crystal growth objectives.

B. Liquid Phase Epitaxial Growth

The LPE layers grown with the pyrolytic graphite slider have, in general, been void-free and specularly reflecting. The growth areas represent a large increase in size compared to an average crystal from a random nucleated solution growth run. Control of layer thickness has been demonstrated by varying the cooldown temperature interval. Generally, thicker layers have

had more irregular surfaces than thinner ones. The exception is LPE run 1 where the cooldown interval was over 300°C; nevertheless, the surface morphology was as good as in most of the runs. The explanation is likely in the more accurately oriented substrates in LPE run 1 [≤1/3 degree from the $(\bar{1}\bar{1}\bar{1})$ plane] compared with ≤1.0 degree from the $(\bar{1}\bar{1}\bar{1})$ plane for all other runs. However, the surface morphology of the LPE layers grown with the pyrolytic graphite slider (No. 2) has not in general been good enough for the fabrication of star sensors for attitude reference systems. To achieve planar LPE growth it is generally believed to be necessary to have a temperature difference across the growth interface in order to prevent constitutional supercooling. The new slider which we have designed and used for LPE-10 and LPE-11 does establish such a temperature difference and has produced the anticipated improvement in surface smoothness. The smoothness of one of the layers has been measured quantitatively and found to exceed 2 μm at only one point over a distance of 12 mm and was generally much less than 1 μm. This measurement is very encouraging but of course the important test of smoothness as well as the other LPE material parameters is photoconductor performance. Photoconductive gain and uniformity measurements (discussed later in this section) on slit detectors formed on LPE-11 layers confirm our selection and development of LPE for larger area, more uniform GaP:Cu photoconductive detectors. We expect continued experiments with the present slider system which explores substrate type, substrate orientation accuracy, growth temperature, and growth interface temperature difference to yield an LPE crystal growth process suitable for star sensor production.

C. Electrical and Optical Properties of GaP

1. Photoconductivity

Discussions of our work on photoconductive effects in GaP:Cu grown from solution by the so-called random nucleation technique have been previously published.[2][3] This subsection discusses the results of the photoconductivity experiments which were performed during this part of the program.

As previously discussed[2] there is a difference between the spectral response for samples fabricated on as-grown, solution-grown GaP:Cu surfaces and that for samples fabricated on interior (i.e., lapped and polished) surfaces. For both types of surfaces there is a rather sharp edge to the low-energy photon response near the energy corresponding to the indirect bandgap in GaP (~2.24 eV). For samples on interior surfaces, the response (i.e., photoconductive gain) falls off for photon energies greater than about 2.8 eV, whereas for samples fabricated on as-grown surfaces the response remains nearly flat out to 4.0 eV. The larger high-energy photon response observed on the as-grown surfaces suggests that the surface recombination rate is lower for these surfaces than it is for the surfaces which have been mechanically or chemically polished. Generally in the random nucleation growth process there exists relatively few as-grown surfaces which are useful for detector fabrication. If the spectral response in the region from 2.8 to 4.0 ev is important, it is desirable to have a growth process which yields a large amount of as-grown surfaces. LPE is, of course, such a process. In Section III we discussed the experiments on the copper doping of GaP during LPE growth.

Early in the program, we elected to determine the potential of LPE for the growth of GaP:Cu as-grown surfaces with the extended short wavelength photoresponse. Figure 21 is a plot of the relative spectral response for one of these samples grown with slider mechanism 2. The fact that the useful response extends to beyond 3.8 eV demonstrated that the LPE process is a useful technique for the growth of GaP:Cu photoconductors with a near-uv response. The peak photoconductive gain measured on this sample was 23. These LPE layers were not highly compensated and, hence, were not optimally doped with copper.

After the growth process was modified, and slider 3 was designed and constructed, additional experiments on the copper doping of GaP during LPE growth were conducted. The spectral dependence of the photoconductive gain for one of these LPE GaP:Cu samples is shown in Fig. 22. For this sample the response has a rather soft leading edge around 2.2 eV (near the indirect band-gap energy of GaP), it reaches a peak just before the direct band gap

energy (~2.8 eV) and then falls off slowly for higher energies. The fact that the gain tails off for photon energies > 2.7 eV suggests that surface recombination is affecting the response. However, the rolloff at energies > 2.8 eV is not nearly as fast as in photoconductive samples fabricated on a lapped and polished surface.

The photoconductive gain, defined as the ratio of lifetime τ to transit time τ_d, in this sample is remarkably high. The gain is dependent on the applied voltage and the geometry of the sample by the relation

$$G = \frac{\tau}{\tau_d} = \frac{\mu \tau V}{\ell^2} \qquad (1)$$

where μ is the mobility, V the applied bias, and ℓ the contact separation. The $\mu\tau$ product is the factor which is important from a materials standpoint. For the sample described in Fig. 22, $\mu\tau \sim 10^{-2}$. If we assume the mobility is 100 cm^2/V-sec we find that the majority carrier lifetime is 10^{-4} sec. This is a long lifetime, indicating that the Cu doping has in fact acted to sensitize the photoconductor. The response time is, of course, ultimately limited by the majority carrier lifetime, so since response times ~ milliseconds are desirable, the lifetime should be $\lesssim 10^{-4}$ sec. Hence from a device standpoint the majority carrier lifetime was nearly optimal.

The resistance of the detector described above was only 520 ohms. Low resistance, of course, gives a high thermal noise current. We have not yet performed a noise analysis on these detectors, but to get an idea of the detection capability of such a device we calculate the minimum detectable power P_{min} assuming that thermal noise is the dominant noise mechanism.

$$P_{min} = \frac{\left(\frac{4kT\Delta f}{R}\right)^{1/2}}{eG} \cdot \left(\frac{I_s}{I_n}\right) \cdot \left|h\nu\right| \qquad (2)$$

In th relation k = Boltzmann's constant, T = temperature, Δf = bandwidth, resistance, e = elementary charge, G = photoconductive gain,

h = Planck's constant, ν = frequency of the radiation, and I_s/I_n = signal-to-noise ratio. If, for example, we require a signal-to-noise ratio of 10 in a 30 Hz bandwidth then for λ = 4600Å, a gain of 2.5×10^4 in a 500-ohm thermal noise limited detector gives a minimum detectable power of 3×10^{-14} watts.

The dependence of the photosignal on the incident photon flux intensity was shown in Fig. 23 in the range from $10^{11} \rightarrow 10^{15}$ photons/cm^2-sec. The linear dependence which is observed at the lower flux intensities is highly desirable from a device standpoint. In the high resistivity (>10^8 ohm-cm) GaP:Cu, grown by the random nucleation solution growth technique, we usually found a superlinear dependence of the signal on the photon flux ($I_s \sim F^2$). [2] In some of the lower-resistivity samples grown by that technique we observed a flux dependence of the signal similar to that shown in Fig. 23. Hence there is now some evidence that the photomechanism in high-resistivity GaP:Cu is not precisely the same as in the low-resistivity material. We need more experimental data from other LPE GaP:Cu photoconductors before attempting a theoretical determination of the photomechanism in material grown by this technique.

Near 10^{-13} photons/cm^2-sec, as shown in Fig. 23, the signal-flux characteristic changes from a linear to a sublinear behavior with the signal varying approximately as $F^{1/2}$. In the literature on sensitized photoconductivity a $F^{1/2}$ dependence is usually attributed to the presence of a distribution in energy of majority carrier traps below the conduction band. The physical picture proposed by Rose[7] to account for sublinear behavior is that as the light intensity is increased the electron demarcation level moves toward the Fermi level and electron traps are converted to recombination centers with a resulting decrease in the majority carrier lifetime. However, preliminary double source photocapacitance data, discussed below, suggests that deep majority carrier trapping effects are minimal in LPE GaP.

We have shown that, in the samples described above, the photosensitivity is decreased by orders of magnitude when the sample is illuminated with radiation of less than band-gap energy. This clearly indicates that a deep acceptor is acting to increase the majority carrier lifetime. We will soon

do a controlled photoquench experiment where the energy of the quenching radiation is systematically varied in order to verify that the sensitizing center (deep acceptor) in the LPE GaP:Cu material is the 0.65 eV Cu level as in all previously Cu-doped GaP.

The spatial uniformity of the photoresponse of a detector fabricated on one of the early LPE GaP:Cu substrates was shown in Fig. 24. This should be compared to Fig. 25 which shows the spatial uniformity of the photosignal for three slits on a recently grown LPE:Cu substrate. The improvement is substantial. The average value and standard deviation for the photosignal for each of these slits is shown in Table 5.

TABLE 5. AVERAGE VALUE, $\bar{x}$, AND STANDARD DEVIATION, S, FOR THE PHOTOSIGNAL IN THREE GaP:Cu PHOTOCONDUCTORS

Slit No.	$\bar{X}$	S
1	.90	0.082
2	.83	0.11
3	.97	0.061

Our goal is to achieve a spatial uniformity in the photoresponse of ±10% over a distance of 5 mm. The data of Fig. 25 indicate that we are very close to achieving that objective.

The frequency dependence of the photosignal for a LPE GaP:Cu photoconductor is shown in Fig. 26. Also shown are the characteristics for response times of 10^{-4} sec and 5×10^{-4} sec. The majority carrier lifetime for this sample was 10^{-4} sec. It is clear that the majority carrier lifetime does not limit the response time. The longer response time is due to the presence of majority carrier traps which to date have not been fully characterized in GaP.

The feasibility of growing sensitized GaP by copper doping has been established. The data that are in indicate that both the sensitivity and spatial uniformity requirements can be achieved. We do not, however, have ample data to establish the reproducibility of the growth process; i.e., how

reproducible is the photoresponse of samples grown under identical conditions, but at different times. We will address this question in the next phase of the program.

During this part of the program the research on the BSG process was directed primarily toward establishing the growth process itself. As discussed above we did not attempt many copper-doping growth runs with this process. The last copper-doped BSG growth run (BSG-18) was substantially improved, from a growth morphology viewpoint, over previous BSG GaP:Cu growth runs; but as of the writing of this report its transport and optical properties had not been evaluated. We did, however, take spectral response data on a few undoped samples and a typical response curve was shown in Fig. 27. The peak of the response occurs near 2.2 eV which is close to the room-temperature indirect bandgap energy (2.24 eV) in GaP. The direct bandgap energy is ~ 2.8 eV for GaP; this accounts for the shoulder in the spectral response. The roll-off in the response at higher energies is due to surface recombination. Note how much faster the photosensitivity declines with increasing photon energy for this sample whose surface has been lapped and polished than it does for a photoconductor fabricated on the as-grown surface of a LPE layer.

2. Transport Measurements

A primary means of identifying and quantitatively measuring the impurities in a semiconductor is by Hall effect measurements. In this subsection we will discuss the information which we have obtained from Hall effect measurements. The Hall data revealed that the first seven BSG growth runs were p-type with the room-temperature carrier concentration varying from 10^{10} cm^{-3} to 10^{17} cm^{-3}. These data also yield an activation energy ~0.042 eV for the shallow acceptor which controls the carrier concentration. These data along with the optical absorption data discussed below strongly suggest that carbon is the impurity in this material which causes it to be p-type. These first seven growth runs used Monsanto polyporous chunk starting material.

To determine whether or not the starting material was responsible for the introduction of carbon in growth run BSG-8 through 17, the starting material was changed to a sulfur-doped Czochralski-grown ingot. Optical absorption experiments on samples from this ingot indicate that carbon is not present in this material. The material from growth runs BSG-8 and -10 was low-resistivity n-type with a carrier concentration in the mid 10^{17} cm^{-3} range. The donor activation energy, as determined from the Hall data, is 0.095 eV, which is the activation energy for sulfur in GaP. The optical absorption data reveal that these two growth runs, which used a starting material free of carbon, still contained a significant carbon concentration (in the 10^{16} cm^{-3} range). From these data we conclude that carbon is inadvertently being introduced during the growth process. A thorough examination of the steps taken during the growth process has not, so far, revealed the source of the contamination.

One of the expected benefits of these two growth processes is an improvement in the uniformity of the material. In Fig. 29 the carrier concentration over $T^{3/2}$ versus reciprocal temperature was plotted for two samples from growth run BSG-10. The fact that the data from each of these samples are equal to within experimental error demonstrates uniformity in majority carrier concentration for this growth run. What we are ultimately interested in, insofar as photoconductor performance is concerned, is uniformity in majority carrier lifetime. The majority carrier lifetime will, however, be determined by the uniformity of the sensitizing centers, i.e., the copper concentration. Therefore, while the material uniformity displayed by the data of Fig. 29 does not conclusively prove that the same spatial uniformity will be observed in the photoresponse of BSG-grown GaP:Cu photoconductors, it certainly encourages us to believe that this technique will yield an improvement in the spatial uniformity of the photoresponse.

The temperature dependence of the electron mobility for a typical n-type BSG sample was shown in Fig. 30. Note that near room temperature the mobility varies approximately as $T^{-3/2}$. Combined intervalley and acoustic mode scattering result in near $T^{-3/2}$ dependence for the electron mobility.[8]

However, the theory predicts a room temperature mobility ~ 200 cm^2/V-sec when these mechanisms limit the mobility. The room temperature mobility for the sample described in Fig. 30 is ~ 110 cm^2/V-sec. The reason for the room temperature mobility being less than 200 cm^2/V-sec is attributed by some authors[9] to ionized impurity scattering. We now briefly discuss the mobility in n-GaP near room temperature.

Rode[10] has shown theoretically that at room temperature ionized impurity scattering can lower the mobility for carrier concentrations $> 10^{17}$ cm^{-3} in uncompensated material and for carrier concentration $\gtrsim 10^{15}$ cm^{-3} in heavily compensated material. He also shows that experiment does not agree with the theory, presumably due to the breakdown of the spherical band approximation in the calculated ionized impurity scattering. Our results show that generally the higher the carrier concentration the lower is the room temperature mobility, but there are exceptions. In Fig. 31 we show the temperature dependence of the mobility for a rather heavily doped uncompensated n-type sample, which should be compared with the data of Fig. 30. Note the mobility of the more heavily doped sample is considerably higher than that for the lighter doped samples. Other investigators have found similar discrepancies. See for example the work of Hara and Akasaki,[11] and Craford, et al.[12] The data suggest that another, yet undetermined, mechanism is influencing the mobility near room temperature. At lower temperatures (< 100°K) the mobility for this n-type BSG-10 sample shown in Fig. 30 varies as $T^{-1/2}$. We have frequently observed this behavior in copper doped GaP. Our preliminary assessment is that the mobility in this region is limited by the scattering of electrons by space charge regions as discussed by Weisberg.[13]

Figure 32 showed a plot of the temperature dependence of the Hall mobility of a typical p-type sample in which carbon is the primary acceptor. Two-phonon scattering gives a temperature dependent mobility which varies as T^{-3}. Likewise, acoustic phonon scattering gives a $T^{-3/2}$ dependence of the mobility. The slopes of a $T^{-3/2}$ and a $T^{-3.0}$ dependence are also shown in Fig. 32. Near room temperature, $\mu \propto T^{-3}$, and around 90°K is asymptotic to $T^{-3/2}$, which suggests the scattering mechanisms mentioned above may limit the mobility. These are, however, not sufficient data to fully determine the scattering mechanisms.

In Fig. 33 we plotted the mobility for an n-type LPE GaP:Cu. This represents our only mobility data for LPE grown material, so we cannot make generalizations. Two points are noteworthy. First, the mobility near room temperature varies as $T^{-3/2}$, but the absolute value is well below the theoretical value for acoustic mode plus intervalley scattering. Secondly the low temperature mobility is quite low. This is to be anticipated since this layer was grown from a gallium solution with 6 percent copper; our past experience[3] is that the low temperature mobility in copper doped samples is quite low.

3. IR Spectroscopy

The most significant result obtained with the optical absorption measurements is the identification of carbon in the BSG samples. As mentioned above, the optical absorption measurements indicate that carbon is being introduced into the crystals during growth. The starting material does not show the presence of carbon, but all of the BSG crystals have an absorption peak at 606 cm^{-1}, characteristic of a carbon local mode line.[14] The concentration is estimated to be between $2.5 \times 10^{16}/cm^3$ and $1 \times 10^{17}/cm^3$, but, as is indicated in Reference 14, this may be in error by as much as a factor of three, with the indications pointing to a higher carbon concentration than estimated by the absorbance measurements.

The oscillatory behavior of the photoconductivity shown in Fig. 36 results from the interaction of the optically excited carriers with the longitudinal optical (LO) phonons. The occurrence of these dips in the photoconductivity can be understood as follows. The onset of extrinsic photoconductivity at low temperatures occurs when the photon energy equals the ionization energy, E_i, of the impurity. As the photon energy increases beyond the ionization energy, the photocurrent per excited carrier generally increases. This is due to the increased lifetime of the optically excited carriers since their probability of capture by the ionized centers decreases as the kinetic energy of the carriers increases. Stocker et al[15] have shown that when the energy of the carriers injected into the band satisfies the condition

$$E(n) = E_i + n\hbar\omega_{LO}, \tag{3}$$

where E(n) is the energy of the carrier, then the injected carriers can decay rapidly to the bottom of the band emitting phonons of energy $\hbar\omega_{LO}$. This results in a decreased average lifetime for the carriers at these injection energies and results in dips in the photoconductivity spectrum.

The ionization energy of the impurity can be obtained from the photoconductivity spectrum using the above expression for the energies of the minima. Plotting the energy of the minimum vs the minimum number, as shown in Fig. 42, we see they form a straight line. The slope of the line is about 400 cm^{-1}, corresponding to the LO phonon frequency in GaP, and the intercept gives an ionization energy of about 400 cm^{-1} (50 meV). The fact that E_i and $\hbar\omega_{LO}$ are approximately the same is purely coincidental. The ionization energy of carbon is reported to be 48 meV[14], so this is consistent with the 50 meV required to give the observed oscillations in the photoconductivity.

4. Junction Capacitance Measurements

It is well known that the majority carrier impurity distribution can be determined from the bias dependence of the junction capacitance. The capacitance of a Schottky barrier on an n-type substrate varies with voltage according to the expression

$$C^{\frac{1}{2}} = 2(\phi_D + V)/(A^2 e\varepsilon_o\epsilon)(N_D - N_A) \tag{4}$$

where A is the area of the junction, e the electron charge, ε_o is the permittivity of free space, ϵ the dielectric constant, $N_D - N_A$ the difference between the ionized donor and acceptor concentrations, ϕ_D the junction diffusion potential, and V the applied bias. Figure 37 showed a typical $1/C^2$ versus V plot at room temperature for a Schottky barrier formed on a BSG substrate. The linear dependence indicates that $N_D - N_A$ does not vary with distance throughout the depletion width of the junction. If we assume that $N_D \gg N_A$ and that all of the donors are ionized at room temperature, these data give a net donor concentration of 1×10^{17} cm^{-3} for this sample. This type of measurement is especially useful in

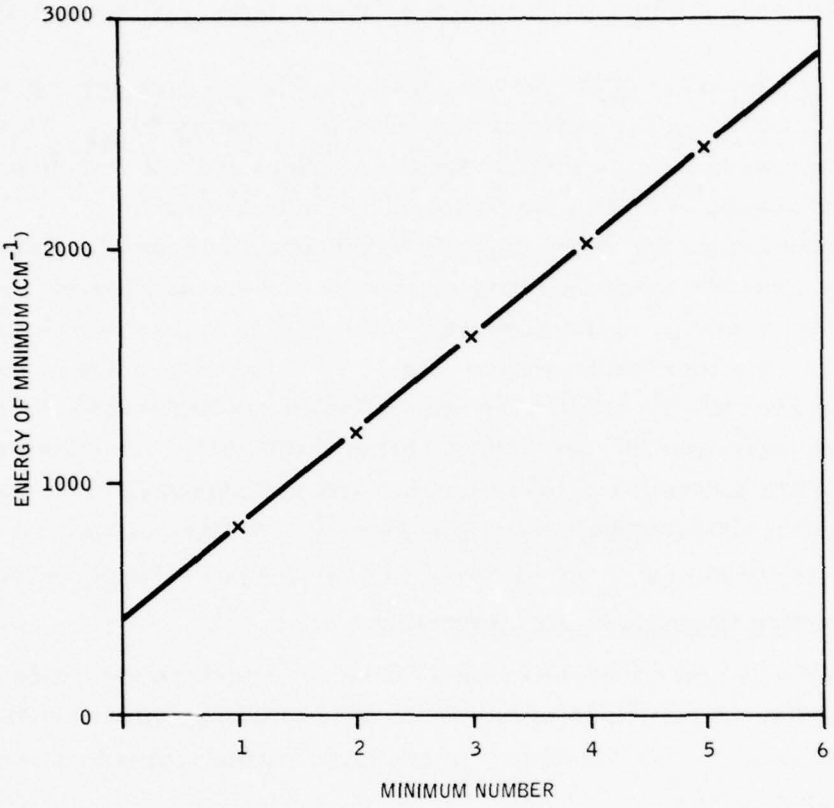

Figure 42. Energy of the photoconductivity minima as a function of the minimum number (the intercept at $400cm^{-1}$ gives the impurity ionization energy).

determining the carrier concentration and type in the LPE-grown layers because it is not easy to fabricate Hall samples from these layers.

$1/C^2$ vs V was plotted in Fig. 38 for three Schottky barriers on an angle-lapped surface of growth LPE 10-63. Diodes Nos. 1, 2 and 3, are approximately 10, 25 and 40 μm below the as-grown surface. Note that the carrier concentration increases with distance from the surface, i. e., the material near the surface is less compensated. This material was inadvertently grown over a large temperature range; the closer to the surface the lower the growth temperature. This suggests, in agreement with our BSG copper doping experiments, that copper is more easily incorporated into GaP at higher than lower temperatures. This is an expected result. The main purpose of presenting these results is to demonstrate the usefulness of C-V measurements for determining carrier concentrations.

Schottky barrier capacitance measurements can also be used for the study and characterization of deep levels in semiconductors. The manner in which deep levels can influence the junction capacitance is illustrated in Fig. 43. Figure 43-a shows the equilibrium band bending and space charge density as a function of distance from the surface in a Schottky barrier formed on an n-type semiconductor with shallow and deep donor levels. When the junction is reversed biased the space charge width, of course, widens with additional states, both shallow and deep, being ionized (see Fig. 43-b). The incremental space charge ΔQ which is introduced by an incremental change ΔV in the potential is shown in the shaded area of Fig. 43-c. In general the capacitance of a planar Schottky diode is given by $\epsilon\epsilon_o A/x_{cg}$, where ϵ is the low-frequency dielectric constant, A the diode area, and x_{cg} the center of gravity of the ΔQ distribution. Hence, if by altering the reverse bias voltage the Fermi level can be moved through the deep defect level, and if the frequency of the ac measuring voltage is low enough so that the population of the deep levels can follow, the deep levels will affect, in some, way, the junction capacitance.

As discussed above we have utilized two techniques for deep level studies in GaP. The first is the Admittance Spectroscopy technique. Figure 39 showed the temperature dependence of the conductance for several frequencies in a GaP/Au Schottky diode which was fabricated on a BSG-4 substrate. The theory for this mechanism predicts that

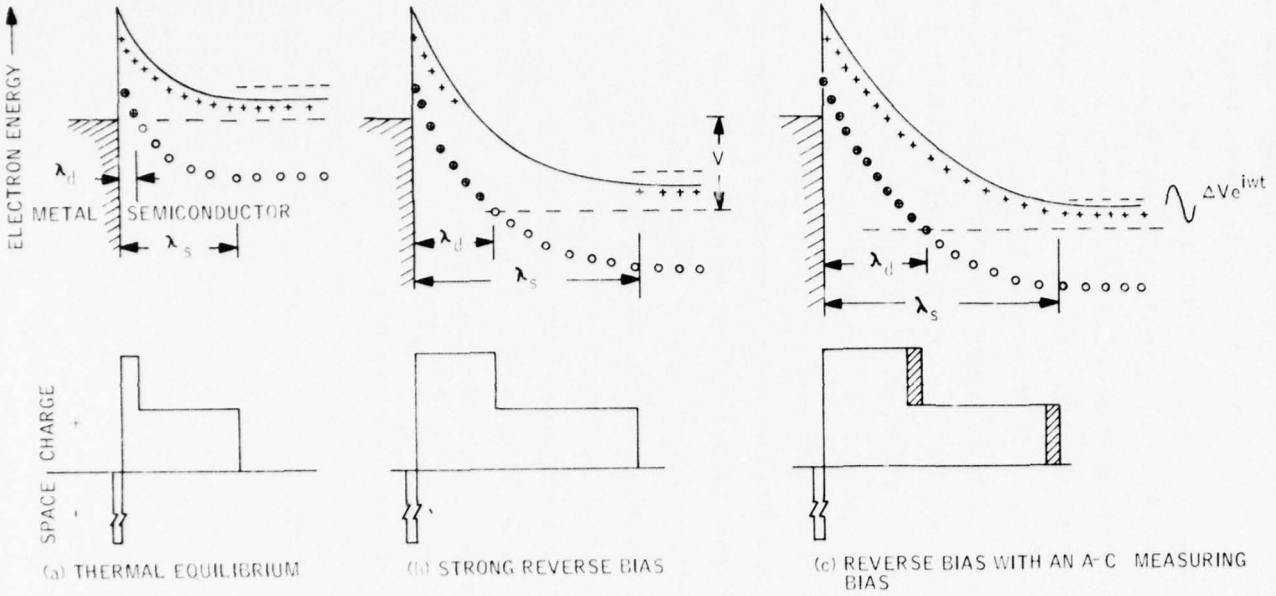

Figure 43. Band schematic of a Schottky barrier and the corresponding space charge distribution for three different bias conditions.

$$\frac{\omega}{T_{peak}^{3/2}} \simeq \exp\left(-\frac{E_t}{KT_{peak}}\right) \qquad (5)$$

where T_{peak} is the temperature of the peak and E_t is the energy depth of the level below the conduction band. In Fig. 44 we have plotted $(\omega)\ (T_{peak})^{-3/2}$ as a function of reciprocal temperature for two samples. The slope of these data give $E_t \simeq 0.14$ eV. Note that one of the points does not fit the straight line. We have not identified the source of this defect.

With the admittance spectroscopy technique we have not been able to identify any other levels in GaP than the one discussed above. In fact, we have encountered difficulty in reproducing results using this technique. We believe that the double-source photocapacitance DSP technique, the results of which are discussed below, is a more useful method for deep-level investigation in GaP. The DSP technique has recently been discussed by White, Dean, and Porteous.[6]

Figure 40 showed the result of our measurement of change in capacitance of Schottky barriers formed on BSG substrates as a function of the probing radiation energy for three different measuring frequencies. These data can be interpreted by assuming a deep donor and a deep acceptor as is shown in Fig. 45. The priming radiation acts to fill the donor levels with electrons and the deep acceptors with holes. When the probe radiation energy is between 0.4 and 0.6 eV, it acts to depopulate the electron traps with a resultant increase in capacitance. At frequencies less than 10^4 Hz and for probe radiation energy greater than 0.6 eV, the capacitance is decreased because the principal effect is to depopulate the hole traps. At the highest frequency (2×10^5 Hz), the capacitance increases monotonically with increasing probe radiation energy. This change in behavior, we believe, is due to the measuring frequency being too high for the deep acceptor to follow. Hence this technique can be used to characterize both the energy location of the defect level and its time constant. Although intentional doping experiments have yet to be done to positively identify the levels, the deep acceptor is most likely copper. The electron trap ($E < 0.4$) is not yet identified.

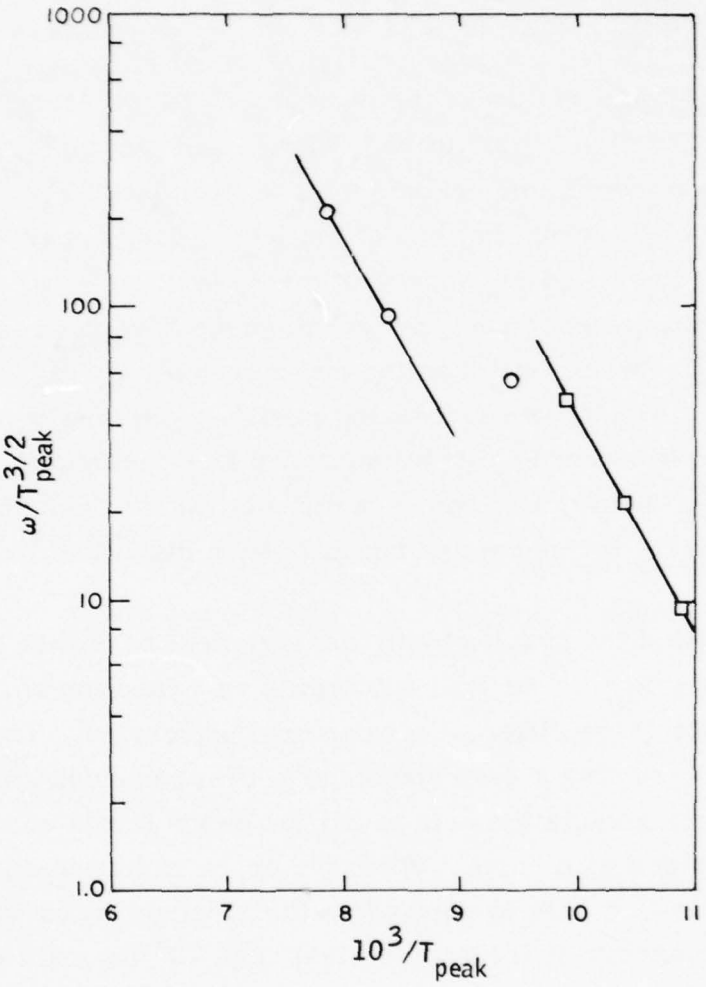

Figure 44. Frequency divided by (temperature)$^{3/2}$ as a function of reciprocal temperature for two Schottky barriers.

AD-A033 640 HONEYWELL CORPORATE RESEARCH CENTER BLOOMINGTON MINN F/G 20/12
ADVANCED DEVELOPMENT ON GALLIUM PHOSPHIDE MATERIALS FOR SATELLI--ETC(U)
MAY 76 P E PETERSEN, R G SCHULZE, M W SCOTT F33615-75-C-5244
UNCLASSIFIED HR-46492 AFML-TR-76-79 NL

2 OF 2
AD-A
033 640

END
DATE
FILMED
1-28-77
NTIS

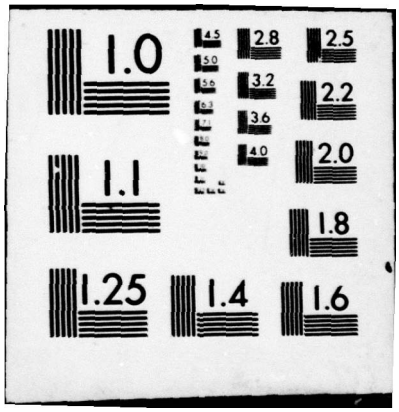
1.0
1.1
1.25
1.4
1.6
2.8
2.5
3.2
2.2
3.6
2.0
4.0
1.8

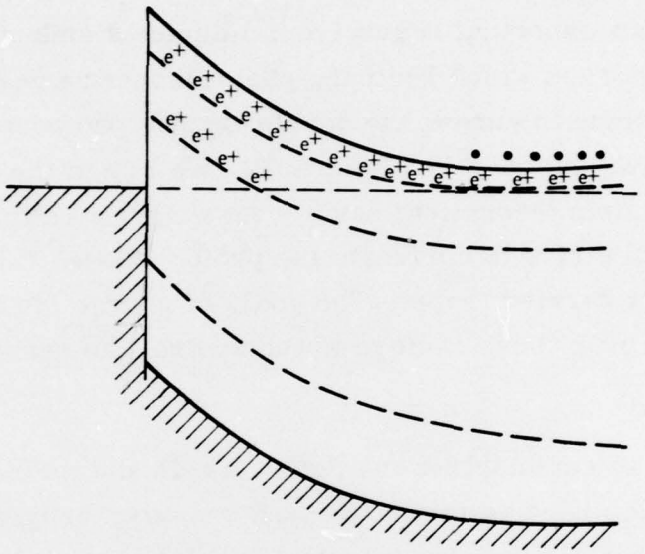

Figure 45. Equilibrium band schematic of a Schottky diode on an n-type substrate with deep donor and acceptor states.

The results of an experiment, similar to that described previously, on a Schottky diode on an LPE layer were shown in Fig. 41. The absence of a capacitive signal for probe radiation < 0.6 eV indicates that majority carrier traps are less prevalent in the LPE layer than in the BSG samples described above. This is an important result from a device standpoint because it is the majority carrier traps which limit the photoconductive response time.

We will continue to pursue the double-source photocapacitance technique as a means of studying deep levels in GaP. We are in the process of putting our results on a firm theoretical basis. As we grow better photoconductive material, we will strive to correlate the photoresponse time with the presence of majority carrier traps. The goal, of course, is to characterize and gain control over those centers which control the response time.

5. Summary

Figure 46 summarizes the defect levels and their activation energies which we have identified so far in our GaP research program. In the future we will work toward better characterization of the deep electron traps and the undesirable acceptors.

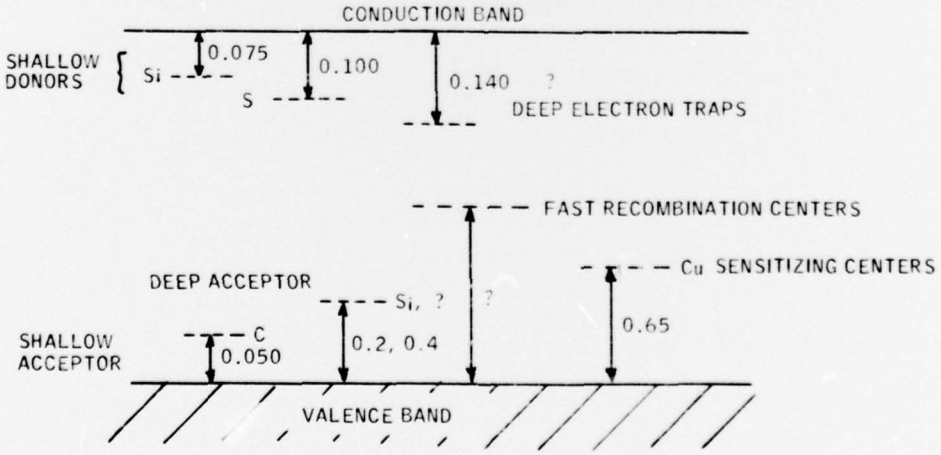

Figure 46. Defect levels in gallium phosphide.

V. PROGRESS AND ACCOMPLISHMENTS

The objective of this research program is to develop a crystal growth program which can produce large, uniform GaP crystals suitable for the high-performance detector applications specified by the Air Force. As discussed earlier, to accomplish this objective we have elected to advance two solution growth techniques for GaP: bulk solution growth and liquid phase epitaxy.

Our research on the growth of GaP and the evaluation of the grown material has proceeded as planned. The BSG apparatus was designed and constructed and has been used to grow large-area (relative to solution growth) single crystals. The design of the growth apparatus in which GaP is synthesized from elemental gallium and phosphorous has been completed. Experiments with this apparatus will begin in the near future.

The LPE apparatus and growth process has been significantly upgraded with a resulting improvement in the quality of the grown layers. Large-area, high-gain, uniform photoconductors have been grown by this technique. The benefits which we anticipated from the further development of the solution growth processes for GaP have been largely realized. The principal problems which we will address in the continuing program are: (1) growth-run to growth-run reproducibility of the photoproperties in the LPE layers, (2) spatial uniformity in BSG GaP:Cu material, (3) advantages of using BSG solution grown substrates for LPE, and (4) characterization of defect levels in solution grown GaP.

Following is an abbreviated list of the significant accomplishments achieved during this program.

- Improved the LPE growth apparatus to achieve:
  - improved surface morphology.
  - increased area of LPE layers to 5mm x 12mm.
- Demonstrated that sensitized copper-doped GaP can be grown by LPE:
  - extended short-wavelength (ultraviolet) response observed on as-grown LPE GaP:Cu layers.

- high-gain sensitized photoconductivity observed in LPE GaP:Cu layers.
- spatial uniformity of photoresponse ~ ±10% observed over 2mm slit length.

- Designed and constructed new growth apparatus for bulk solution growth.
  - large-area single crystals grown by BSG technique.
  - growth rate ~ 1 mm/day achieved.
  - uniformity of majority carrier concentration in BSG GaP < 10%.
  - control over temperature profile permits further crystal size improvement.

- Advanced materials evaluation capability for GaP.
  - employed Fourier Transform spectroscopy for defect studies in GaP.
  - employed oscillatory photoconductivity for defect studies in GaP.
  - utilized double source photocapacitance technique for deep level studies in GaP.
  - developed van der Pauw and high resistivity capability for Hall and resistivity studies in GaP.

REFERENCES

1. H. Nakatsuka, A. J. Domenico and G. L. Pearson, Solid-State Electron. 14, 849 (1971).

2. R. G. Schulze and P. E. Petersen, J. Appl. Phys. 45, 5307 (1974).

3. P. E. Petersen (to be submitted for publication).

4. Hayes, W., MacDonald, H. F., and Sennett, C. T., J. Phys. C. 2 2402 (1969).

5. D. L. Losee, J. Appl. Phys. 46, 2204 (1975).

6. A. M. White, P. J. Dean and P. Porteous, J. Appl. Phys. 47, 3230 (1976).

7. A. Rose, Concepts in Photoconductivity and Allied Problems, Interscience, New York (1963).

8. M. Toyama, M. Naito, and A. Kasami, Jap. J. Appl. Phys. 8 358 (1969).

9. K. Gillessen and A. J. Marshall, J. Crystal Growth 32, 216 (1976).

10. D. L. Rode, Phys. Stat. Sol 53, 245 (1972).

11. T. Hara and I. Akasaki; J. Appl. Phys. 39, 285 (1968).

12. M. G. Craford, W. O. Groves, A. H. Herzog, and D. E. Hill, J. Appl Phys. 42, 2751 (1971).

13. L. R. Weisberg, J. Appl. Phys. 5, 1817 (1962).

14. F. Thompson and R. C. Newman, J. Phys. C 4, 3249 (1971).

15. H. J. Stocker, H. Levinstein, C. R. Stannard, Phys. Rev. 150, 613 (1966).

☆ U. S. GOVERNMENT PRINTING OFFICE: 1976 — 757-001/25